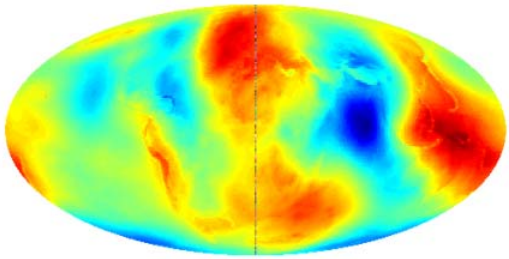

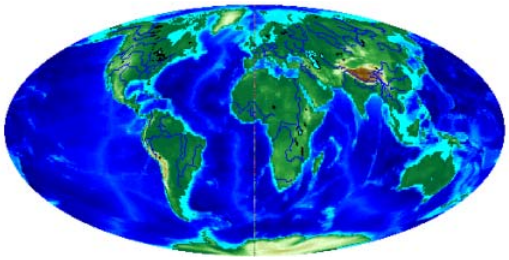

Siegen Preprints on Geomathematics

Spline Multiresolution and Numerical Results for Joint Gravitation and Normal Mode Inversion With an Outlook on Sparse Regularisation

P. Berkel D. Fischer V. Michel

Geomathematics Group Siegen

www.geomathematics-siegen.de

1

Spline Multiresolution and Numerical Results for Joint Gravitation and Normal Mode Inversion With an Outlook on Sparse Regularisation

Paula Berkel Doreen Fischer Volker Michel *

February 11, 2010

Abstract

Numerical results of a spline regularisation technique for the determination of the mass density distribution in the Earth based on a joint inversion of gravitational and normal mode data are presented. Gravitational data yields many typical mass anomalies in the Earth's crust, whereas no deep features can be recovered from it. However, normal mode data reveals certain structures in the Earth's mantle, although also this inversion suffers from a non-uniqueness problem. The joint inversion requires a weighting process to avoid a strong dominance of the gravitational data. Finally, an outlook on a sparse regularisation is given.

Keywords: inverse problem, regularisation, tomography, crust, mantle, inverse gravimetry, normal modes, reproducing kernel, spline, sparse regularisation

AMS 2000 Classification: 86A22, 65R32, 46E22, 65D07.

1 Introduction

One of the fundamental problems in the geosciences is the investigation of the Earth's interior. Three-dimensional Earth models are needed e.g. for the detection of hidden resources or for precise earthquake localisation and source characterisation. Knowledge of the density distribution within the mantle provides important information about the Earth's dynamics, such as plate motions, convection and geochemistry (see e.g. [17, 47, 50]).
A well-known ansatz for the determination of the Earth's density is the inverse gravimetric problem, i.e. the inversion of Newton's gravitational potential

$$V(x) = \gamma \int_{\mathscr{B}} \frac{\rho(y)}{|x-y|} \, \mathrm{d}y \, , \tag{1}$$

where γ is the gravitational constant, $\mathscr{B}$ is an approximation of the Earth and ρ is the unknown density. The present satellite missions CHAMP, GRACE, and GOCE provide us with models of the gravitational

*Geomathematics Group, Department of Mathematics, University of Siegen, Walter-Flex-Str. 3, 57068 Siegen, Germany; e-mail: fischer@mathematik.uni-siegen.de, michel@mathematik.uni-siegen.de

field which have an unprecedented precision. However, the inversion of the integral operator in (1) is non-unique since the null-space of the operator consists of all anharmonic functions on $\mathscr{B}$ (see e.g. the survey article [45]). This means that only the harmonic part of the density can be calculated from the gravitational potential. As a matter of fact, the harmonic density of a spherically symmetric Earth model is a constant function. Since the structures in the deep interior of the Earth are primarily spherically symmetric, one cannot obtain any reasonable density model from gravitational data alone. As a consequence, also other types of data, e.g. from seismology, have to be considered.

One possible approach in seismology is the examination of the Earth's normal modes. After major earthquakes, the whole Earth oscillates for a relatively long period of time. These vibrations are called the free oscillations or the normal modes of the Earth. Their analysis gives us knowledge about the structure of the Earth's interior.

Today modern networks can easily record free oscillations from earthquakes with surface wave magnitudes greater than about 6.5. There are roughly 20 such events per year such that now many thousands of recordings are available for normal mode research.

For each normal mode, there exists an associated splitting function, which corresponds to a local average of the Earth's three-dimensional heterogeneity. More precisely, the value of the splitting function at a particular direction $\xi \in \Omega$ (with Ω being the unit sphere) can be interpreted as the degenerate frequency perturbation that the mode would experience if the spherically averaged Earth structure was identical to the structure in the direction ξ.

There is a known relation between the splitting functions and the isotropic material properties of the Earth, which can be described by three independent parameters. These are, for instance, the compressional velocity α, the shear velocity β and the density ρ. Usually, density models are obtained by scaling a compressional or shear velocity model. However, the assumption of a simple relationship between the velocities and the density is questionable when lateral variations are a result of non-thermal effects, i.e. chemical heterogeneity (see e.g. [16, 38]). However, it is still a controversial discussion between seismologists if the current data situation is sufficient for the computation of independent density models. Independent models are presented e.g. in [28, 29, 30, 58], whereas their validity is denied in [33, 40, 57, 61].

In this paper, we want to combine normal mode data with gravitational data in order to obtain more detailed information about the Earth's density distribution than we get from the gravitational data alone. Especially in regions below the Earth's crust, the harmonic solution of the inverse gravimetric problem provides us only with poor information due to the maximum principle.

Note that an ansatz for the combined inversion of normal modes and gravity anomalies is presented in [28, 29]. Therein, the authors use the spherical harmonic coefficients of the splitting functions and of the free air gravity anomalies to construct a combined system of linear equations. The solution is expanded laterally in spherical harmonics and radially in Chebyshev polynomials. Then the system is solved by a damped least-squares inversion where the damping guarantees that the solution is similar to a certain starting model.

Here, we will use localised spline basis functions which are based on certain reproducing kernel Hilbert spaces. The resulting spline provides us with a preferably smooth solution of the interpolation problem, which is the best approximation to the unknown function. Recent applications of related techniques can be found e.g. in [1, 2, 4, 5, 15, 32, 46].

In addition, we construct a combination of the spline interpolation technique with features of a multiresolution analysis. Note that the techniques presented here are not only suitable for normal mode and

inverse gravimetry but also for other problems with a similar structure.
In the following, an outline of this paper is given.
After a summary of a few notations and basic fundamentals in Section 2, Section 3 gives a short overview of the geoscientific problems we are interested in, i.e. normal mode tomography and inverse gravimetry. We introduce the necessary quantities and formulae and present some important theoretical properties of the problems. In particular, the representation of the available data as the values of functionals applied to the unknown functions is investigated, since such formulae are essential for the construction of the spline method later on.
In Section 4, the used (scalar and vectorial) spline method is briefly explained. One great advantage of this method is that we are able to combine different types of data, e.g. seismic and gravitational data, into one system of linear equations. Among all interpolating functions this spline has minimal Sobolev norm (first minimum property), which guarantees a certain smoothness of the solution such that the name "spline" is justified. Furthermore, the interpolating spline is the unique best approximation of a given function F in the spline space (second minimum property).
In Section 5, we combine the presented spline interpolation method with features of a multiresolution analysis. For this purpose, we construct a sequence of Sobolev spaces in such a way that the "hat-width" of the corresponding reproducing kernels decreases with increasing scale. At each step, we add more data in order to obtain a better resolution. The resulting sequence of interpolating splines converges to the unknown function. This multiresolution technique can be applied to the scalar and to the vectorial case in a similar manner.
In Section 6, the spline method is applied to the geoscientific problems introduced in Section 3. In particular, the general form of the occurring systems of linear equations and of the resulting splines is derived.
In Section 7, we present some numerical results. We start with the inversion of a purely gravitational dataset which gives us the harmonic density of the Earth. Then we carry out inversions of both synthetic and genuine normal mode data. At last, we consider a combined inversion of normal mode and gravitational data and discuss the occurring problems.
In Section 8, we give an outlook on a matching pursuit technique as an alternative method providing us with sparsity of the solution and an enhanced zooming-in. First numerical results for the application to the inverse gravimetric problem are given.
Finally, Section 9 summarises the results of this work and gives an outlook for further research.

2 Preliminaries

There are two known $\mathrm{L}^2(\mathscr{B})$-orthonormal systems on the ball $\mathscr{B} := \{x \in \mathbb{R}^3 \mid |x| = a\}$, which are denoted by $\{G^{\mathrm{I}}_{m,n,j}\}_{m,n\in\mathbb{N}_0;\, j=1,\dots,2n+1}$ and $\{G^{\mathrm{II}}_{m,n,j}\}_{m,n\in\mathbb{N}_0;\, j=1,\dots,2n+1}$ in [44], where the upper reference "I" or "II" is omitted if both systems may be used. For the numerical results presented in this paper, only system I was used:

$$G^{\mathrm{I}}_{m,n,j}(x) := \sqrt{\frac{4m+2n+3}{a^3}}\, P_m^{(0,n+\frac{1}{2})}\left(2\frac{|x|^2}{a^2}-1\right)\left(\frac{|x|}{a}\right)^n Y_{n,j}\left(\frac{x}{|x|}\right),$$

where $\{P_m^{(\alpha,\beta)}\}_{m\in\mathbb{N}_0}$ represents the Jacobi polynomials (corresponding to the parameters $(\alpha,\beta) \in]-1,\infty[^2$) and $\{Y_{n,j}\}_{n=0,1,\dots;\, j=1,\dots,2n+1}$ represents an orthonormal $\mathrm{L}^2(\Omega)$-basis of spherical harmonics (Ω is

the unit sphere in $\mathbb{R}^3$). This system is based on [3, 9]. Fourier coefficients with respect to a chosen basis system will be denoted by $F^\wedge(m,n,j) := (F, G_{m,n,j})_{\mathrm{L}^2(\mathscr{B})}$. Note that a represents the radius of the Earth. Moreover, if X and Y are Banach spaces, then $\mathscr{L}(X,Y)$ represents the Banach space of all bounded linear operators $A : X \to Y$.

3 Theoretical Aspects of the Involved Inverse Problems

3.1 Normal Mode Tomography

After major earthquakes, the whole Earth oscillates for a long time. These vibrations are called the free oscillations or the normal modes. The corresponding eigenfrequencies can be obtained by a Fourier analysis of long period seismograms and have values approximately between 0.3 and 20 mHz. For each normal mode, one can calculate a unique splitting function from the spatially varying difference between the measured eigenfrequencies of the Earth and the eigenfrequencies calculated for a given Earth model. The splitting functions correspond to a local average of the Earth's 3D-structure and, therefore, reveal information about the density inside the Earth.

3.1.1 Splitting Functions

The free oscillations of the Earth can be divided into two main groups: spheroidal (or poloidal) modes, denoted by ${}_kS_l$, and toroidal (or torsional) modes, denoted by ${}_kT_l$. (Note that in the literature we usually find the notation ${}_nS_l$ and ${}_nT_l$.) Each displacement field is related to a spherical harmonic of degree l, i.e. $Y_{l,m},\ m \in \{1,\dots,2l+1\}$. If we consider a spherically symmetric, non-rotating Earth model, the frequency of a certain mode is independent of the order m of the corresponding spherical harmonic. Therefore, we have $2l+1$ modes with the same (degenerate) frequency. These $2l+1$ modes are called the singlets and are combined into one multiplet. Since the real Earth is not spherically symmetric, each singlet has a slightly different frequency. This phenomenon is named the "splitting".
Each multiplet has its own unique splitting function σ. The value of the splitting function at a particular direction $\xi \in \Omega$ can be interpreted as the degenerate frequency perturbation that the multiplet would experience if the spherically averaged Earth structure was identical to the structure in the direction ξ.
There are different methods for estimating splitting functions from the data spectra, e.g. iterative spectral fitting ([26, 27, 56, 59, 60]), receiver stripping ([39, 40]) and peak shift observation ([31, 64, 68]). Several research groups provide splitting function coefficients on the internet, usually with respect to fully normalised spherical harmonics. For an overview and more information, we refer the reader to the "Reference Earth Model Website" ([54]). For the application of a localised technique it would, of course, be more advantageous to have data with a spatial reference (frequency shifts could be an alternative, see also [4]).
Since the splitting function σ (corresponding to one fixed multiplet) only depends on the direction $\xi \in \Omega$, it can be regarded as an element of $\mathrm{L}^2(\Omega)$. It, thus, can be expanded as $\sigma = \sum_{n=0}^{\infty}\sum_{j=1}^{2n+1}\sigma^\wedge(n,j)Y_{n,j}$. Its coefficients $\sigma^\wedge(n,j)$, $n \in \mathbb{N}_0$, $j \in \{1,\dots,2n+1\}$, are related to the material properties of the Earth by

$$\sigma^\wedge(n,j) = \int_0^a \mathbf{k}_n(r) \cdot \left(\delta\mathbf{m}^\wedge(n,j)\right)(r)\,\mathrm{d}r\ , \tag{1}$$

where $\delta\mathbf{m} := (\frac{\delta\alpha}{\alpha_{\mathrm{M}}}, \frac{\delta\beta}{\beta_{\mathrm{M}}}, \frac{\delta\rho}{\rho_{\mathrm{M}}})$ represents the relative deviation of the compressional velocity, the shear

velocity and the mass density from the spherically symmetric reference model $(\alpha_{\mathrm{M}}, \beta_{\mathrm{M}}, \rho_{\mathrm{M}})$ (usually PREM). Note that

$$\left(\left(\delta\mathbf{m}^{\wedge}(n,j)\right)(r)\right)_i = \left((\delta\mathbf{m}(r\cdot))_i, Y_{n,j}\right)_{\mathrm{L}^2(\Omega)}, \quad i = 1,2,3.$$

Furthermore, $\mathbf{k}_n := (K_n^{\alpha}, K_n^{\beta}, K_n^{\rho})$, $n \in \mathbb{N}_0$, are the corresponding sensitivity kernels (see e.g. [6, 36, 69]).

Remark 3.1 A radial integration similar to that in equation (1) also occurs in the context of the inverse problems in gravimetry (see [45, 48, 52, 62]) and magnetoencephalography (MEG, see [13, 14]).

A linear functional mapping $(\delta\alpha, \delta\beta, \delta\rho)$ to $\sigma(\xi_k) \in \mathbb{R}$, $\xi_k \in \Omega$, can be defined by

$$\begin{aligned} \mathscr{F}_{\mathrm{Sp}}^{k}(\delta\alpha, \delta\beta, \delta\rho) := \sigma(\xi_k) &= \sum_{n=0}^{\infty} \sum_{j=1}^{2n+1} \sigma^{\wedge}(n,j) Y_{n,j}(\xi_k) \\ &= \sum_{n=0}^{\infty} \sum_{j=1}^{2n+1} \int_0^a \hat{\mathbf{k}}_n(r) \cdot \left((\delta\alpha, \delta\beta, \delta\rho)^{\wedge}(n,j)\right)(r)\, \mathrm{d}r\, Y_{n,j}(\xi_k)\,, \end{aligned} \tag{2}$$

where

$$\hat{\mathbf{k}}_n := \left(\frac{K_n^{\alpha}}{\alpha_{\mathrm{M}}}, \frac{K_n^{\beta}}{\beta_{\mathrm{M}}}, \frac{K_n^{\rho}}{\rho_{\mathrm{M}}}\right).$$

3.2 Inverse Gravimetry

The relation between the gravitational potential V and the mass density distribution ρ is given by Newton's Law of Gravitation

$$V(x) = \gamma \int_{\mathscr{B}} \frac{\rho(y)}{|x-y|}\, \mathrm{d}y\,, \quad x \in \mathbb{R}^3 \setminus \mathscr{B}\,, \tag{3}$$

where γ is the gravitational constant. It is a well-known fact that only the harmonic part of the density distribution can be obtained from the gravitational potential.

Theorem 3.2 *The operator $T : \mathrm{L}^2(\mathscr{B}) \to T(\mathrm{L}^2(\mathscr{B}))$, given by*

$$(TF)(x) := \int_{\mathscr{B}} \frac{F(y)}{|x-y|}\, \mathrm{d}y\,, \quad x \in \mathbb{R}^3 \setminus \mathscr{B}\,,$$

has the null-space

$$\ker T = \mathrm{Anharm}(\mathscr{B}) := \left\{ F \in \mathrm{L}^2(\mathscr{B}) \,\middle|\, (F,H)_{\mathrm{L}^2(\mathscr{B})} = 0 \text{ for all } H \in \mathrm{C}^{(2)}(\mathscr{B}) \text{ with } \Delta H = 0 \right\}.$$

This theorem was proven in [51, 52, 34] (in chronological order of the steps leading eventually to this result). The result can also be found e.g. in [9, 49, 67].

Modern satellite techniques like SST (satellite-to-satellite tracking), which is used in case of the satellites CHAMP ([24, 53]) and GRACE ([10, 25]), and SGG (satellite gravity gradiometry), which is applied in case of the mission GOCE ([10, 11, 63]), yield data from which derivatives of the gravitational potential can be deduced. The relevant types of functionals, which map $\rho \in \mathrm{L}^2(\mathscr{B})$ to $\mathbb{R}$, are:

- gravitational potential:

$$\mathscr{F}_0^k \rho := \int_{\mathscr{B}} \frac{\rho(y)}{|x_k - y|} \, \mathrm{d}y \,, \quad x_k \in \mathbb{R}^3 \setminus \mathscr{B} \text{ fixed}, \tag{4}$$

- (negative) first radial derivative:

$$\mathscr{F}_1^k \rho := -\left(\frac{x}{|x|} \cdot \nabla_x \int_{\mathscr{B}} \frac{\rho(y)}{|x-y|} \, \mathrm{d}y \right) \Bigg|_{x=x_k}, \quad x_k \in \mathbb{R}^3 \setminus \mathscr{B} \text{ fixed},$$

- second radial derivative:

$$\mathscr{F}_2^k \rho := \left(\frac{x}{|x|} \cdot \left(\left(\nabla_x \otimes \nabla_x \int_{\mathscr{B}} \frac{\rho(y)}{|x-y|} \, \mathrm{d}y \right) \frac{x}{|x|} \right) \right) \Bigg|_{x=x_k}, \quad x_k \in \mathbb{R}^3 \setminus \mathscr{B} \text{ fixed}.$$

We obtain for $\rho \in \mathrm{L}^2(\mathscr{B})$ the representation (cf. [23, 42, 43])

$$\mathscr{F}_i^k \rho = \sum_{n=0}^{\infty} \sum_{j=1}^{2n+1} q_n^{(i)} \frac{4\pi}{2n+1} \sqrt{\frac{a^3}{2n+3}} \left(\rho, G_{0,n,j}^{\mathrm{I}} \right)_{\mathrm{L}^2(\mathscr{B})} \left(\frac{a}{|x_k|} \right)^n \frac{1}{|x_k|} Y_{n,j} \left(\frac{x_k}{|x_k|} \right) , \tag{5}$$

where

$$q_n^{(i)} := \begin{cases} 1, & i = 0 \\ \frac{n+1}{|x_k|}, & i = 1 \\ \frac{(n+1)(n+2)}{|x_k|^2}, & i = 2 \end{cases} .$$

Note that it is also possible to derive an expansion of the gravitational potential in terms of the basis of type II, see [5].
If we want to apply the functionals to the density deviation $\delta\rho = \rho - \rho_{\mathrm{M}}$ we have to calculate the gravitational potential $\tilde{V}$ associated to this deviation, i.e.

$$\tilde{V}(x) := \int_{\mathscr{B}} \frac{\delta\rho(y)}{|x-y|} \, \mathrm{d}y = \int_{\mathscr{B}} \frac{\rho(y) - \rho_{\mathrm{M}}(y)}{|x-y|} \, \mathrm{d}y = V(x) - (T\rho_{\mathrm{M}})(x) \,, \quad x \in \mathbb{R}^3 \setminus \mathscr{B} \,.$$

Since a spherically symmetric model will be chosen for ρ_{M}, we can define $\hat{\rho}_{\mathrm{M}} : [0,a] \to \mathbb{R}$ by

$$\hat{\rho}_{\mathrm{M}}(r) = \hat{\rho}_{\mathrm{M}}(|x|) := \rho_{\mathrm{M}}(x) \quad \text{for all } x = r\xi \in \mathscr{B} \,.$$

In [41], it is shown that $T\rho_{\mathrm{M}}$ is given by

$$(T\rho_{\mathrm{M}})(x) = \frac{4\pi}{|x|} \int_0^a r^2 \hat{\rho}_{\mathrm{M}}(r) \, \mathrm{d}r \,,$$

hence,

$$\tilde{V}(x) = V(x) - \frac{4\pi}{|x|} \int_0^a r^2 \hat{\rho}_{\mathrm{M}}(r) \, \mathrm{d}r$$

for all $x \in \mathbb{R}^3 \setminus \mathscr{B}$. In case of the Earth model PREM, $T\rho_{\mathrm{M}}$ is (approximately) given by

$$(T\rho_{\mathrm{M}})(x) = \frac{4\pi a^3}{3|x|} \cdot 5.5134 \, \frac{\mathrm{g}}{\mathrm{cm}^3} \, .$$

It should be noted that the inversion of $\rho \mapsto V$ (with the requirement of a harmonic solution ρ for the uniqueness) is ill-posed, i.e. instable, since the singular values of $\rho \mapsto V$ converge to 0 (see (5)) and the operator is, consequently, compact. Note that this convergence is exponential if the potential is not given at the Earth's surface but above it (exponential ill-posedness of the downward continuation problem).

4 Splines

In this section, a brief summary of the construction of scalar and vectorial splines for the investigated problems is given. For further details, the reader is referred to [4, 5, 44]. An advantage of these spline methods is the possibility to combine different types of data (e.g. seismic and gravitational data) into one interpolation problem. The vectorial approach is, for example, appropriate for the simultaneous determination of $\delta\alpha$, $\delta\beta$, and $\delta\rho$ and the treatment of the corresponding coupled problem.

4.1 Sobolev Spaces

Let $\{A_{m,n}\} := \{A_{m,n}\}_{m,n\in\mathbb{N}_0}$ be a real sequence. Consider the set $\mathscr{E} := \mathscr{E}(\{A_{m,n}\};\mathscr{B})$ of all functions $F \in \mathrm{L}^2(\mathscr{B})$ of the form

$$F = \sum_{m=0}^{\infty} \sum_{n=0}^{\infty} \sum_{j=1}^{2n+1} F^{\wedge}(m,n,j) G_{m,n,j} \, , \tag{6}$$

satisfying

$$F^{\wedge}(m,n,j) = 0 \quad \text{for all } m,n \in \mathbb{N}_0 \text{ with } A_{m,n} = 0 \tag{7}$$

and

$$\sum_{\substack{m,n=0 \\ A_{m,n}\neq 0}}^{\infty} \sum_{j=1}^{2n+1} A_{m,n}^{-2} \left(F^{\wedge}(m,n,j)\right)^2 < +\infty \, .$$

We can define an inner product $(\cdot,\cdot)_{\mathscr{H}(\{A_{m,n}\};\mathscr{B})}$ on $\mathscr{E}$ by

$$(F,G)_{\mathscr{H}(\{A_{m,n}\};\mathscr{B})} := \sum_{\substack{m,n=0 \\ A_{m,n}\neq 0}}^{\infty} \sum_{j=1}^{2n+1} A_{m,n}^{-2} F^{\wedge}(m,n,j) \, G^{\wedge}(m,n,j) \, .$$

The Sobolev space $\mathscr{H}(\{A_{m,n}\};\mathscr{B})$ is defined as the completion of $\mathscr{E}(\{A_{m,n}\};\mathscr{B})$ with respect to the inner product $(\cdot,\cdot)_{\mathscr{H}(\{A_{m,n}\};\mathscr{B})}$. $\mathscr{H}(\{A_{m,n}\};\mathscr{B})$ equipped with the inner product $(\cdot,\cdot)_{\mathscr{H}(\{A_{m,n}\};\mathscr{B})}$ is a Hilbert space. Note that the Sobolev space $\mathscr{H}(\{1\};\mathscr{B})$ is equal to the space $\mathrm{L}^2(\mathscr{B})$.
Further on, we write $\mathscr{H}$ instead of $\mathscr{H}(\{A_{m,n}\};\mathscr{B})$ if no confusion is likely to arise.
Note that we always assume that the chosen sequence $\{A_{m,n}\}$ is summable with respect to the basis of type I, i.e.

$$\sum_{m=0}^{\infty} \sum_{n=0}^{\infty} A_{m,n}^2 \, n(2m+n) \binom{m+n+\frac{1}{2}}{m}^2 < +\infty \, . \tag{8}$$

The summability of the sequence $\{A_{m,n}\}$ automatically guarantees that every element of $\mathscr{H}(\{A_{m,n}\};\mathscr{B})$ can be related to a continuous bounded function. Moreover, it implies the existence of the reproducing kernel

$$K_{\mathscr{H}}(x,y) = \sum_{m=0}^{\infty}\sum_{n=0}^{\infty}\sum_{j=1}^{2n+1} A_{m,n}^2 G_{m,n,j}(x)G_{m,n,j}(y)\ , \quad x,y\in\mathscr{B}\ ,$$

of $\mathscr{H}$. For the discussion of examples and criteria for the fulfilment of the summability condition see [4, 22].

4.2 Scalar Splines

By means of the reproducing kernels, we define splines in $\mathscr{H}$ corresponding to a system of bounded linear functionals.

Definition 4.1 *Let $N\in\mathbb{N}$ and let $\mathscr{F} := \{\mathscr{F}^1,\dots,\mathscr{F}^N\}\subset\mathscr{L}(\mathscr{H},\mathbb{R})$ be a linearly independent system of bounded linear functionals from $\mathscr{H}$ into $\mathbb{R}$. A function $S\in\mathscr{H}$ of the form*

$$S(x) = \sum_{k=1}^{N} a_k \mathscr{F}^k K_{\mathscr{H}}(\cdot,x)\ , \quad x\in\mathscr{B}\ , \tag{9}$$

$a=(a_1,\dots,a_N)^{\mathrm{T}}\in\mathbb{R}^N$, is called a spline in $\mathscr{H}$ relative to $\mathscr{F}$. Spline$(\mathscr{H};\mathscr{F})$ *represents the space of all such splines.*

For further consideration, we need the following lemma which can also be found in [7].

Lemma 4.2 *Let $\mathscr{F}\in\mathscr{L}(\mathscr{H},\mathbb{R})$ be arbitrary. Then $y\mapsto\mathscr{F}_x K_{\mathscr{H}}(x,y)$ is in $\mathscr{H}$ and*

$$\mathscr{F}F = \left(F,\mathscr{F}_x K_{\mathscr{H}}(x,\cdot)\right)_{\mathscr{H}}$$

for all $F\in\mathscr{H}$.

Here, $\mathscr{F}_x K_{\mathscr{H}}(x,y)$ means that $\mathscr{F}$ is applied to the function $x\mapsto K_{\mathscr{H}}(x,y)$, where y is arbitrary but fixed. A spline interpolation problem can be formulated as follows: Let there be given a linearly independent system of functionals $\mathscr{F} := \{\mathscr{F}^1,\dots,\mathscr{F}^N\}\subset\mathscr{L}(\mathscr{H},\mathbb{R})$, $N\in\mathbb{N}$, and a vector $b=(b_1,\dots,b_N)^{\mathrm{T}}\in\mathbb{R}^N$. Determine $S\in$ Spline$(\mathscr{H};\mathscr{F})$ such that

$$\mathscr{F}^i S = b_i \quad \text{for all } i=1,\dots,N$$

or, equivalently, determine $a\in\mathbb{R}^N$ such that

$$\sum_{j=1}^{N} a_j \mathscr{F}_y^i \mathscr{F}_x^j K_{\mathscr{H}}(x,y) = b_i \quad \text{for all } i=1,\dots,N\,.$$

As a consequence, the spline interpolation problem corresponds to a system of linear equations with the matrix

$$\left(\mathscr{F}_y^i\mathscr{F}_x^j K_{\mathscr{H}}(x,y)\right)_{i,j=1,\dots,N}\ , \tag{10}$$

which is (as a Gramian matrix) positive definite.
Hence, the spline interpolation problem is uniquely solvable. Moreover, it is known that the obtained spline has certain nice properties such as maximal smoothness (first minimum property), i.e.

$$\begin{aligned} & S \in \text{Spline}(\mathscr{H};\mathscr{F}) \text{ with } \mathscr{F}^i S = b_i \text{ for all } i = 1,\dots,N \\ & \quad \Leftrightarrow \quad S \in \mathscr{H} \text{ with } \|S\|_{\mathscr{H}} \le \|F\|_{\mathscr{H}} \text{ for all } F \in \mathscr{H} \text{ with } \mathscr{F}^i F = \mathscr{F}^i S = b_i \text{ for all } i = 1,\dots,N, \end{aligned} \tag{11}$$

and best approximation (second minimum property), see [4, 44].

4.3 Vectorial Splines

As we mentioned above, models involving simple relationships between the velocities and the mass density are disputed. For this reason, we will not use such a simplification. As a consequence, we have to solve the coupled problem based on (1). Since this requires the simultaneous determination of the three independent quantities $(\delta\alpha, \delta\beta, \delta\rho)$ (although our primary intention is still to find $\delta\rho$ only), we need vectorial splines. Vectorial splines on the sphere were introduced in [19, 20, 21]. These splines are based on vector spherical harmonics, i.e. they can be separated in normal and tangential parts. Since we are looking for a vector of three independent functions, we will define here a component based method. The method is based on the scalar technique above and will only briefly be explained here. For further details, see [4, 5].

Definition 4.3 *Let $\mathscr{H}_1, \mathscr{H}_2, \mathscr{H}_3$ be three scalar Sobolev spaces as introduced in Section 4.1. The spaces may differ with respect to the chosen symbol $\{A_{m,n}\}$ and the used basis $\{G^{\mathrm{I/II}}_{m,n,j}\}$. We consider the space $\mathfrak{H} := \mathscr{H}_1 \times \mathscr{H}_2 \times \mathscr{H}_3$ and we define an inner product on $\mathfrak{H}$ by*

$$(f,g)_{\mathfrak{H}} := (F_1,G_1)_{\mathscr{H}_1} + (F_2,G_2)_{\mathscr{H}_2} + (F_3,G_3)_{\mathscr{H}_3} \ ,$$

where $f := (F_1,F_2,F_3)$ and $g := (G_1,G_2,G_3)$ are elements of $\mathfrak{H}$.

Obviously, $(\cdot,\cdot)_{\mathfrak{H}}$ is an inner product on $\mathfrak{H}$ since $(\cdot,\cdot)_{\mathscr{H}_i}$ is an inner product on $\mathscr{H}_i$ for $i = 1,2,3$. Moreover, $(\mathfrak{H},(\cdot,\cdot)_{\mathfrak{H}})$ is complete. Note that the data will now be represented by functionals $\mathscr{F} \in \mathscr{L}(\mathfrak{H},\mathbb{R})$.
We will now define a tensorial kernel $\mathfrak{K}$, which inherits some reproducing kernel properties from the scalar kernels $K_{\mathscr{H}_i}$, $i = 1,2,3$.

Definition 4.4 *Let $K_{\mathscr{H}_i} : \mathscr{B} \times \mathscr{B} \to \mathbb{R}$ be the unique reproducing kernel of $\mathscr{H}_i$, $i = 1,2,3$. The tensorial kernel $\mathfrak{K} : \mathscr{B} \times \mathscr{B} \to \mathbb{R}^{3\times 3}$ corresponding to $\mathfrak{H}$ is defined by*

$$\mathfrak{K}(x,y) := \begin{pmatrix} K_{\mathscr{H}_1}(x,y) & 0 & 0 \\ 0 & K_{\mathscr{H}_2}(x,y) & 0 \\ 0 & 0 & K_{\mathscr{H}_3}(x,y) \end{pmatrix}, \quad x,y \in \mathscr{B}.$$

Note that if we choose one parameter $x \in \mathscr{B}$ arbitrary but fixed, each row of $\mathfrak{K}(\cdot,x)$ is an element of $\mathfrak{H}$, since $K_{\mathscr{H}_i}(\cdot,x)$ is an element of $\mathscr{H}_i$, $i = 1,2,3$. Therefore, we can apply a functional $\mathscr{F} \in \mathscr{L}(\mathfrak{H},\mathbb{R})$ row-wise:

$$\mathscr{F}\mathfrak{K}(\cdot,x) := \begin{pmatrix} \mathscr{F}(K_{\mathscr{H}_1}(\cdot,x)\,,\,0\,,\,0) \\ \mathscr{F}(0\,,\,K_{\mathscr{H}_2}(\cdot,x)\,,\,0) \\ \mathscr{F}(0\,,\,0\,,\,K_{\mathscr{H}_3}(\cdot,x)) \end{pmatrix}.$$

This property can be used for the definition of splines in $\mathfrak{H}$.

Definition 4.5 *Let $N \in \mathbb{N}$ and let $\mathscr{F} := \{\mathscr{F}^1, \ldots, \mathscr{F}^N\} \subset \mathscr{L}(\mathfrak{H}, \mathbb{R})$ be a linearly independent system of bounded linear functionals from $\mathfrak{H}$ into $\mathbb{R}$. A function $s \in \mathfrak{H}$ of the form*

$$s(x) = \sum_{k=1}^{N} a_k \mathscr{F}^k \mathfrak{K}(\cdot, x) \;, \quad x \in \mathscr{B} \;, \tag{12}$$

$a = (a_1, \ldots, a_N)^{\mathrm{T}} \in \mathbb{R}^N$, is called a (vectorial) spline in $\mathfrak{H}$ relative to $\mathscr{F}$. Such splines are collected in the space $\mathrm{spline}(\mathfrak{H}; \mathscr{F})$.

A spline interpolation problem can be formulated in analogy to the scalar case: A system of linearly independent functionals $\mathscr{F} := \{\mathscr{F}^1, \ldots, \mathscr{F}^N\} \subset \mathscr{L}(\mathfrak{H}, \mathbb{R})$, $N \in \mathbb{N}$, and a vector $b = (b_1, \ldots, b_N)^{\mathrm{T}} \in \mathbb{R}^N$ are given. Determine $s \in \mathrm{spline}(\mathfrak{H}; \mathscr{F})$ such that

$$\mathscr{F}^i s = b_i \quad \text{for all } i = 1, \ldots, N$$

or, equivalently, determine $a \in \mathbb{R}^N$ such that

$$\sum_{j=1}^{N} a_j \mathscr{F}_y^i \mathscr{F}_x^j \mathfrak{K}(x, y) = b_i \quad \text{for all } i = 1, \ldots, N \,. \tag{13}$$

Obviously, (13) represents a system of linear equations with the matrix

$$\left(\mathscr{F}_y^i \mathscr{F}_x^j \mathfrak{K}(x, y)\right)_{i,j=1,\ldots,N} \;, \tag{14}$$

which is positive definite.
Analogous properties can be proved for the vectorial splines, such as the maximal smoothness property (see (11)) and the best approximation property.

5 Spline Multiresolution

In this section, we combine the introduced spline method with a multiresolution concept. The concept is explained in detail for the scalar splines and can be established in an analogous manner for the vectorial splines (see [4, 5] for further details). The principle is as follows: We construct different sequences $\{A_{m,n}^{(J)}\}$ (which will now be called $\{\Phi_J^\wedge(m,n)\}$) corresponding to different scales J such that we obtain a sequence of approximating splines at increasing scales. At each step, we add more data and reduce the "hat-width" of the spline basis functions in order to obtain a better resolution. Our approach is based on the spline-wavelet method in [12, 46]. The proofs are partially analogous. Alternative spline-wavelet approaches for different geomathematical problems can be found in [18, 22].

Notation 5.1 In this section, the following notations are used: Let $\mathscr{F}$ represent a given, fixed, and countable system of linear and continuous functionals $\mathscr{F} = \left\{\mathscr{F}^1, \mathscr{F}^2, \ldots\right\} \subset \mathscr{L}(\mathscr{H}, \mathbb{R})$. Moreover, let $\mathscr{F}_{(N_J)} = \left\{\mathscr{F}^1, \ldots, \mathscr{F}^{N_J}\right\} \subset \mathscr{F}$ be a linearly independent subsystem and $b^{(J)} \in \mathbb{R}^{N_J}$ be a given vector for every $J \in \mathbb{N}_0$, where $(N_J)_{J \in \mathbb{N}_0}$ is a monotonically increasing sequence of positive integers with $\lim\limits_{J \to \infty} N_J = +\infty$.

Definition 5.2 *Let the family of sequences* $\{\Phi_J^\wedge(m,n)\}_{m,n\in\mathbb{N}_0}$, $J\in\mathbb{N}_0$, *satisfy the conditions*

(i) $0\le\Phi_J^\wedge(m,n)\le\Phi_{J+1}^\wedge(m,n)\le 1$ *for all* $J\in\mathbb{N}_0$, $m,n\in\mathbb{N}_0$,

(ii) $\{\Phi_J^\wedge(m,n)\}_{m,n\in\mathbb{N}_0}$ *is summable for all* $J\in\mathbb{N}_0$ *(see (8)),*

(iii) for all fixed $m,n\in\mathbb{N}_0$, *the sequence* $\{\Phi_J^\wedge(m,n)\}_{J\in\mathbb{N}_0}$ *is not identical to* 0, *i.e. (in combination with condition (i)) there exists* $j_{m,n}$ *such that* $\Phi_J^\wedge(m,n)>0$ *for all* $J\ge j_{m,n}$.

Furthermore, let

$$\mathscr{H}_J := \mathscr{H}\left(\left\{\Phi_J^\wedge(m,n)\right\};\mathscr{B}\right)\ .$$

Then the elements of $\mathrm{Spline}(\mathscr{H}_J;\mathscr{F}_{(N_J)})$ *are called spline scaling functions.*

Figure 1 shows the third component of the spline basis function $\mathscr{F}_{\mathrm{Gr}}^k\mathfrak{K}(\cdot,y)$ at a sphere with $|y|=6365\,\mathrm{km}$ corresponding to a data point satisfying $|x_k|=6371\,\mathrm{km}$ (see Section 6 for further details). Here, the symbol of the CP-scaling function was used which is defined by

$$\Phi_J^\wedge(m,n) := \begin{cases} 0, & \text{if} \quad 2m+n\ge 2^J \\ \left(1-2^{-J}(2m+n)\right)\left(1+2^{1-J}(2m+n)\right)^{1/2}, & \text{if} \quad 2m+n<2^J \end{cases}\ . \tag{15}$$

The figure shows that the "hat-width" decreases with increasing scale.
The Sobolev spaces $\mathscr{H}_J$, $J\in\mathbb{N}_0$, defined by the symbol $\{\Phi_J^\wedge(m,n)\}$ represent a multiresolution analysis as the following theorem shows.

Theorem 5.3 *Let* $\{\Phi_J^\wedge(m,n)\}_{m,n\in\mathbb{N}_0}$, $J\in\mathbb{N}_0$, *satisfy the conditions of Definition 5.2. Then the Sobolev spaces* $\mathscr{H}_J$ *form a multiresolution analysis, i.e.*

(i) $\mathscr{H}_0\subset\ldots\subset\mathscr{H}_J\subset\mathscr{H}_{J+1}\subset\ldots\subset\mathscr{H}_\infty \quad$ *for all* $J\in\mathbb{N}_0$,

(ii) $\overline{\bigcup\limits_{J\in\mathbb{N}_0}\mathscr{H}_J}^{\|\cdot\|_{\mathscr{H}_\infty}}=\mathscr{H}_\infty$,

where $\mathscr{H}_\infty := \mathscr{H}\left(\{\varphi(m,n)\};\mathscr{B}\right)$ *and* $\varphi(m,n):=\lim\limits_{J\to\infty}\Phi_J^\wedge(m,n)$ *for all* $m,n\in\mathbb{N}_0$.

Proof. We first mention that, for fixed $m,n\in\mathbb{N}_0$, the sequence $\{\Phi_J^\wedge(m,n)\}_{J\in\mathbb{N}_0}$ is monotonically increasing, bounded and, therefore, convergent. Moreover, the third requirement in Definition 5.2 implies in combination with the monotonicity that this limit $\varphi(m,n)$ is positive for each (m,n).

(i) Let $F\in\mathscr{H}_J$ be an arbitrary element of the Sobolev space at scale $J\in\mathbb{N}_0$. Hence, the condition

$$\sum_{\substack{m,n=0\\ \Phi_J^\wedge(m,n)\neq 0}}^{\infty}\sum_{j=1}^{2n+1}\Phi_J^\wedge(m,n)^{-2}\left(F^\wedge(m,n,j)\right)^2<+\infty$$

must be satisfied. Because of the monotonicity of the symbol, we conclude that

$$\sum_{\substack{m,n=0\\ \Phi_{J+1}^\wedge(m,n)\neq 0}}^{\infty}\sum_{j=1}^{2n+1}\Phi_{J+1}^\wedge(m,n)^{-2}\left(F^\wedge(m,n,j)\right)^2\le\sum_{\substack{m,n=0\\ \Phi_J^\wedge(m,n)\neq 0}}^{\infty}\sum_{j=1}^{2n+1}\Phi_J^\wedge(m,n)^{-2}\left(F^\wedge(m,n,j)\right)^2<+\infty\,, \tag{16}$$

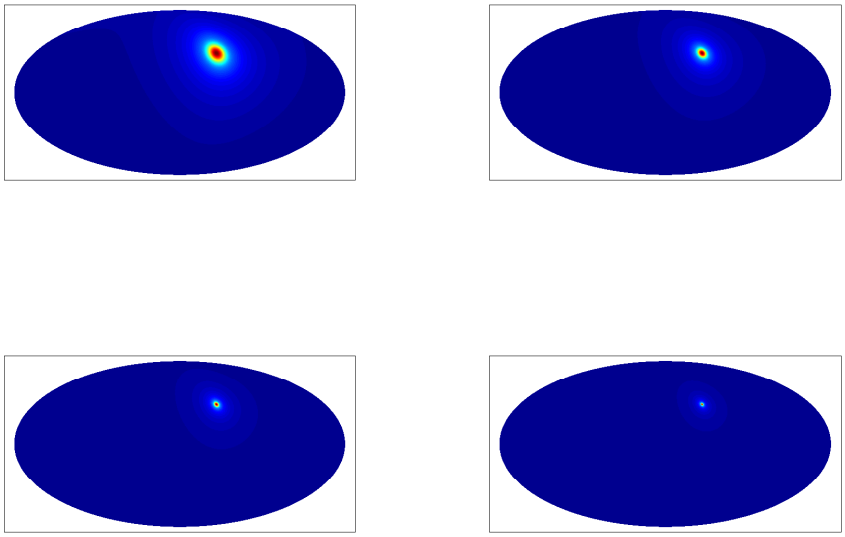

Figure 1: Plots of the third component of the spline basis function $\mathscr{F}^k_{\mathrm{Gr}}\mathfrak{K}(\cdot,y)$ with respect to the CP-scaling function at scales $J=5$ (top left-hand), $J=6$ (top right-hand), $J=7$ (bottom left-hand), and $J=8$ (bottom right-hand)

such that $F \in \mathscr{H}_{J+1}$. Note that

$$F^\wedge(m,n,j)=0 \text{ for all } (m,n) \in \left\{(p,q) \in \mathbb{N}_0 \times \mathbb{N}_0 \,\middle|\, \Phi^\wedge_J(p,q)=0\right\} \supset \left\{(p,q) \in \mathbb{N}_0 \times \mathbb{N}_0 \,\middle|\, \Phi^\wedge_{J+1}(p,q)=0\right\}$$

due to condition (7).
In analogy, we obtain that $F \in \mathscr{H}_\infty$, since $\varphi(m,n) \geq \Phi^\wedge_J(m,n)$.

(ii) Now, let $F \in \mathscr{H}_\infty$ be arbitrary. Hence, by definition, F satisfies

$$\sum_{m=0}^{\infty}\sum_{n=0}^{\infty}\sum_{j=1}^{2n+1}\frac{1}{\varphi(m,n)^2}\left(F^\wedge(m,n,j)\right)^2 < +\infty\,. \tag{17}$$

After defining the sequence $\{H_J\}_{J\in\mathbb{N}_0}$ of functions by

$$H_J := \sum_{m=0}^{\infty}\sum_{n=0}^{\infty}\sum_{j=1}^{2n+1}\frac{\Phi^\wedge_J(m,n)}{\varphi(m,n)}F^\wedge(m,n,j)\,G_{m,n,j}\,,$$

we observe that $H_J \in \mathscr{H}_J$ for all $J \in \mathbb{N}_0$, since

$$\|H_J\|^2_{\mathscr{H}_J} = \sum_{\substack{m,n=0\\ \Phi^\wedge_J(m,n)\neq 0}}^{\infty}\sum_{j=1}^{2n+1}\frac{1}{\Phi^\wedge_J(m,n)^2}\frac{\Phi^\wedge_J(m,n)^2}{\varphi(m,n)^2}\left(F^\wedge(m,n,j)\right)^2 \leq \sum_{m=0}^{\infty}\sum_{n=0}^{\infty}\sum_{j=1}^{2n+1}\frac{1}{\varphi(m,n)^2}\left(F^\wedge(m,n,j)\right)^2 < +\infty\,.$$

Moreover, we observe that the series of the Parseval identity

$$\begin{aligned}\|F-H_J\|^2_{\mathscr{H}_\infty} &= \left\| \sum_{m=0}^{\infty}\sum_{n=0}^{\infty}\sum_{j=1}^{2n+1}\left(1-\frac{\Phi_J^\wedge(m,n)}{\varphi(m,n)}\right)F^\wedge(m,n,j)\,G_{m,n,j}\right\|^2_{\mathscr{H}_\infty}\\ &= \sum_{m=0}^{\infty}\sum_{n=0}^{\infty}\sum_{j=1}^{2n+1}\varphi(m,n)^{-2}\left(1-\frac{\Phi_J^\wedge(m,n)}{\varphi(m,n)}\right)^2\left(F^\wedge(m,n,j)\right)^2\end{aligned}$$

converges uniformly with respect to $J\in\mathbb{N}_0$ due to estimate (17) and the fact that $0\le\frac{\Phi_J^\wedge(m,n)}{\varphi(m,n)}\le 1$. Consequently, we get

$$\lim_{J\to\infty}\|F-H_J\|^2_{\mathscr{H}_\infty}=\sum_{m=0}^{\infty}\sum_{n=0}^{\infty}\sum_{j=1}^{2n+1}\varphi(m,n)^{-2}\lim_{J\to\infty}\left(1-\frac{\Phi_J^\wedge(m,n)}{\varphi(m,n)}\right)^2\left(F^\wedge(m,n,j)\right)^2=0\ .$$

This implies the second property of the multiresolution. ∎

Furthermore, inequality (16) yields the following corollary.

Corollary 5.4 *Let $J\in\mathbb{N}_0$ and let $F\in\mathscr{H}_J$ be an arbitrary function. Then*

$$\|F\|_{\mathscr{H}_{J+1}}\le\|F\|_{\mathscr{H}_J}\ .$$

By means of Theorem 5.3, we can construct a sequence of approximating splines $S_J\in\mathrm{Spline}(\mathscr{H}_J;\mathscr{F}_{(N_J)})$. Each spline S_J is the smoothest function in the space $\mathscr{H}_J$ that interpolates the given data, i.e. $\mathscr{F}^i S_J=b_i^{(J)}$, $i=1,\dots,N_J$. Since the symbol $\{\Phi_J^\wedge(m,n)\}_{m,n\in\mathbb{N}_0}$ increases with respect to J by definition, the corresponding reproducing kernels become more and more localised (see also Figure 1). This involves that the resolution increases and, thus, more and more data has to be included ($N_J\le N_{J+1}$).
If we additionally require $\varphi(m,n)=1$ in Theorem 5.3, it directly follows that the "limit space" $\mathscr{H}_\infty$ is the space $\mathrm{L}^2(\mathscr{B})$.
Finally, we get a system of linear equations for each scale. The approximating spline at scale $J\in\mathbb{N}_0$ can be calculated by solving the system of linear equations given by

$$\sum_{k=1}^{N_J}a_k^{(J)}\mathscr{F}_y^i\mathscr{F}_x^k K_{\mathscr{H}_J}(x,y)=b_i^{(J)}\ ,\quad i=1,\dots,N_J\,.$$

The corresponding spline has the representation

$$S_J(x)=\sum_{k=1}^{N_J}a_k^{(J)}\mathscr{F}^k K_{\mathscr{H}_J}(\cdot,x)\ ,\quad x\in\mathscr{B}\ .$$

By adding more and more data and decreasing the "hat-width" of the basis functions at the same time, we obtain a sequence of approximating splines. We want to show now that this sequence converges to the unknown function of our interpolation problem. However, before we can prove this convergence we need some lemmata. Their proofs are analogous to proofs in [12]. We omit them for this reason.

Lemma 5.5 *The dual spaces $\mathscr{H}_J^* := \mathscr{L}(\mathscr{H}_J, \mathbb{R})$, satisfy*

$$\mathscr{H}_\infty^* \subset \mathscr{H}_{J+1}^* \subset \mathscr{H}_J^* \subset \mathscr{H}_0^*$$

for all $J \in \mathbb{N}_0$. Furthermore,

$$\|\mathscr{T}\|_{\mathscr{H}_0^*} \leq \|\mathscr{T}\|_{\mathscr{H}_J^*} \leq \|\mathscr{T}\|_{\mathscr{H}_{J+1}^*} \leq \|\mathscr{T}\|_{\mathscr{H}_\infty^*}$$

for all $\mathscr{T} \in \mathscr{H}_\infty^*$.

Lemma 5.6 *For all $F \in \mathscr{H}_j$, $j \in \mathbb{N}_0$, we have*

$$\lim_{\substack{J\to\infty \\ J\geq j}} \|F\|_{\mathscr{H}_J} = \|F\|_{\mathscr{H}_\infty} \ .$$

Theorem 5.7 (Convergence Theorem) *Let $F \in \bigcup_{J\in\mathbb{N}_0} \mathscr{H}_J$ be a given function, $\mathscr{F} = \{\mathscr{F}^i\}_{i\in\mathbb{N}}$ be a linearly independent system of linear and continuous functionals in $\mathscr{H}_\infty^*$ such that* $\operatorname{span}\{\mathscr{F}^i\}_{i\in\mathbb{N}}$ *is dense in $\mathscr{H}_\infty^*$. Let there exist subsystems $\mathscr{F}_{(N_J)} := \{\mathscr{F}^1, \ldots, \mathscr{F}^{N_J}\} \subset \mathscr{F}$, $J \in \mathbb{N}_0$, with $N_J \leq N_{J+1}$ for all $J \in \mathbb{N}_0$ and $\lim_{J\to\infty} N_J = +\infty$. Moreover, let the sequence of spline scaling functions $(S_J)_{J\in\mathbb{N}_0}$ be given by*

$$\begin{aligned} S_J &\in \operatorname{Spline}\left(\mathscr{H}_J; \mathscr{F}_{(N_J)}\right) \ , \\ \mathscr{F}^i S_J &= \mathscr{F}^i F \text{ for all } i = 1, \ldots, N_J \ . \end{aligned} \tag{18}$$

Then

$$\lim_{J\to\infty} \|S_J - F\|_{\mathscr{H}_\infty} = 0 \ . \tag{19}$$

Proof. We prove property (19) for $F \in \mathscr{H}_j$ for an arbitrary but fixed scale $j \in \mathbb{N}_0$. For this purpose, we show in part a) that S_J converges weakly to F with respect to $(\cdot,\cdot)_{\mathscr{H}_\infty}$. After that, we prove in part b) that $\lim_{J\to\infty} \|S_J\|_{\mathscr{H}_\infty} = \|F\|_{\mathscr{H}_\infty}$ to obtain, in the end, the assumed result. For a related harmonic spherical case without multiresolution we refer the reader to [18].

a) Let $\mathscr{T} \in \mathscr{H}_\infty^*$ be arbitrary. We have to show that $\mathscr{T} S_J \to \mathscr{T} F$ as $J \to \infty$. Let $\varepsilon > 0$ be given. Since $\operatorname{span}\{\mathscr{F}^i\}_{i\in\mathbb{N}}$ is dense in $\mathscr{H}_\infty^*$, there exists a finite linear combination

$$\tilde{\mathscr{T}} = \sum_{i=1}^{N} b_i \mathscr{F}^i \in \mathscr{H}_\infty^* \ (\subset \mathscr{H}_J^* \text{ for all } J \in \mathbb{N}_0) \ ,$$

$N \in \mathbb{N}$, such that

$$\left\|\mathscr{T} - \tilde{\mathscr{T}}\right\|_{\mathscr{H}_\infty^*} \leq \varepsilon \ . \tag{20}$$

Now let J_0 be sufficiently large such that $N_{J_0} \geq N$ and $J_0 \geq j$. Then we have for all $J \geq J_0$ due to (18)

$$\tilde{\mathscr{T}} S_J = \sum_{i=1}^{N} b_i \mathscr{F}^i S_J = \sum_{i=1}^{N} b_i \mathscr{F}^i F = \tilde{\mathscr{T}} F \ .$$

Hence, Lemma 4.2 and the Cauchy-Schwarz inequality imply that

$$\begin{aligned} |\mathscr{T}S_J - \mathscr{T}F| &= \left|\left(\mathscr{T}-\tilde{\mathscr{T}}\right)(S_J - F)\right| \\ &= \left|\left(S_J - F, \left(\mathscr{T}-\tilde{\mathscr{T}}\right)_x K_{\mathscr{H}_J}(x,\cdot)\right)_{\mathscr{H}_J}\right| \\ &\leq \|S_J - F\|_{\mathscr{H}_J} \left\|\left(\mathscr{T}-\tilde{\mathscr{T}}\right)_x K_{\mathscr{H}_J}(x,\cdot)\right\|_{\mathscr{H}_J} \\ &\leq \left(\|S_J\|_{\mathscr{H}_J} + \|F\|_{\mathscr{H}_J}\right) \left\|\left(\mathscr{T}-\tilde{\mathscr{T}}\right)_x K_{\mathscr{H}_J}(x,\cdot)\right\|_{\mathscr{H}_J} \end{aligned} \tag{21}$$

for all $J \geq J_0$. Using again Lemma 4.2, we obtain the estimate

$$\begin{aligned} \left\|\left(\mathscr{T}-\tilde{\mathscr{T}}\right)_x K_{\mathscr{H}_J}(x,\cdot)\right\|^2_{\mathscr{H}_J} &= \left(\left(\mathscr{T}-\tilde{\mathscr{T}}\right)_x K_{\mathscr{H}_J}(x,\cdot), \left(\mathscr{T}-\tilde{\mathscr{T}}\right)_x K_{\mathscr{H}_J}(x,\cdot)\right)_{\mathscr{H}_J} \\ &= \left(\mathscr{T}-\tilde{\mathscr{T}}\right)_y \left(\mathscr{T}-\tilde{\mathscr{T}}\right)_x K_{\mathscr{H}_J}(x,y) \\ &\leq \left\|\mathscr{T}-\tilde{\mathscr{T}}\right\|_{\mathscr{H}_J^*} \left\|\left(\mathscr{T}-\tilde{\mathscr{T}}\right)_x K_{\mathscr{H}_J}(x,\cdot)\right\|_{\mathscr{H}_J} , \end{aligned}$$

such that we get with Lemma 5.5

$$\left\|\left(\mathscr{T}-\tilde{\mathscr{T}}\right)_x K_{\mathscr{H}_J}(x,\cdot)\right\|_{\mathscr{H}_J} \leq \left\|\mathscr{T}-\tilde{\mathscr{T}}\right\|_{\mathscr{H}_J^*} \leq \left\|\mathscr{T}-\tilde{\mathscr{T}}\right\|_{\mathscr{H}_\infty^*} .$$

Putting this result into inequality (21), we can conclude from (11), (20), and Corollary 5.4 that for all $J \geq J_0$

$$|\mathscr{T}S_J - \mathscr{T}F| \leq 2\|F\|_{\mathscr{H}_J} \left\|\mathscr{T}-\tilde{\mathscr{T}}\right\|_{\mathscr{H}_\infty^*} \leq 2\|F\|_{\mathscr{H}_J}\,\varepsilon \leq 2\|F\|_{\mathscr{H}_j}\,\varepsilon .$$

Hence,

$$\lim_{J\to\infty} \mathscr{T}S_J = \mathscr{T}F \quad \text{for all } \mathscr{T} \in \mathscr{H}_\infty^* .$$

b) Without loss of generality, we may assume that $F \neq 0$, since otherwise $\|S_J\|_{\mathscr{H}_j} \leq \|F\|_{\mathscr{H}_j}$ (see (11)) implies that $S_J = 0$ for all $J\ \big(\geq j\big)$. Furthermore, we may assume, without loss of generality, that a given value $\varepsilon > 0$ is sufficiently small such that $0 < \varepsilon < \|F\|_{\mathscr{H}_j}$. According to a well-known fact from functional analysis (see e.g. [70], p. 91), we have

$$\|F\|_{\mathscr{H}_\infty} = \sup_{\substack{\mathscr{T}\in \mathrm{span}\{\mathscr{F}^i\}_{i\in\mathbb{N}} \\ \|\mathscr{T}\|_{\mathscr{H}_\infty^*}\leq 1}} |\mathscr{T}F| .$$

Therefore, we can find a functional

$$\tilde{\mathscr{T}} = \sum_{i=1}^{N} d_i \mathscr{F}^i \in \mathscr{H}_\infty^* \ (\subset \mathscr{H}_J^* \text{ for all } J \in \mathbb{N}_0)$$

with $\|\tilde{\mathscr{T}}\|_{\mathscr{H}_\infty^*} \leq 1$ and $\|F\|_{\mathscr{H}_\infty} \leq |\tilde{\mathscr{T}}F| + \varepsilon$. Moreover, due to Corollary 5.4 and Lemma 5.6, there exists $J_0 \geq j$ such that for all $J \geq J_0$ the inequality

$$0 \leq \|F\|_{\mathscr{H}_J} - \|F\|_{\mathscr{H}_\infty} \leq \varepsilon$$

holds. Thus, if we choose J_1 such that $J_1 \geq J_0$ and $N_{J_1} \geq N$, we obtain for all $J \geq J_1$, using Corollary 5.4 and (11),

$$\begin{aligned} \|F\|_{\mathscr{H}_\infty} &\leq \left|\tilde{\mathscr{T}}F\right| + \varepsilon = \left|\tilde{\mathscr{T}}S_J\right| + \varepsilon \leq \left\|\tilde{\mathscr{T}}\right\|_{\mathscr{H}_\infty^*} \|S_J\|_{\mathscr{H}_\infty} + \varepsilon \leq \|S_J\|_{\mathscr{H}_\infty} + \varepsilon \\ &\leq \|S_J\|_{\mathscr{H}_J} + \varepsilon \leq \|F\|_{\mathscr{H}_J} + \varepsilon \leq \|F\|_{\mathscr{H}_\infty} + 2\varepsilon \end{aligned}$$

such that

$$\lim_{J\to\infty} \|S_J\|_{\mathscr{H}_\infty} = \|F\|_{\mathscr{H}_\infty} .$$

Combining a) and b), we see that

$$\lim_{J\to\infty} \|S_J - F\|_{\mathscr{H}_\infty} = 0$$

for all $F \in \bigcup_{J\in\mathbb{N}_0} \mathscr{H}_J$. ∎

Remark 5.8 It is enough to find a sufficiently large $j \in \mathbb{N}_0$ such that $F \in \mathscr{H}_j$, where $\bigcup_{J\in\mathbb{N}_0} \mathscr{H}_J$ is dense in $\mathscr{H}_\infty$. Consequently, we have, in practice, a sufficiently large set of approximable functions.

6 Application of the Spline Method to the Combined Inverse Problem

In this chapter, we give some details about the application of the derived spline methods to the inverse problems introduced in Chapter 3.
We consider functionals that map $(\delta\alpha, \delta\beta, \delta\rho) \in (\mathrm{L}^2(\mathscr{B}))^3$ to a real number. The given data will be a mixture of splitting function values and anomalies in the gravitational potential. For the normal mode tomography, we have the functional given by (2). For the inverse gravimetric problem, we choose the functional corresponding to the gravitational potential based on (4):

$$\mathscr{F}^k_{\mathrm{Gr}}(\delta\alpha, \delta\beta, \delta\rho) := \int_{\mathscr{B}} \frac{\delta\rho(y)}{|x_k - y|} \mathrm{d}y .$$

$\{\xi_k\}_k \subset \Omega$ and $\{x_k\}_k \subset \mathbb{R}^3 \setminus \mathscr{B}$ are point grids on which the corresponding data is given. Note that the gravitational potential is usually given either shortly above the Earth's surface or at a satellite orbit.
Application of the functionals to the basis functions in $\mathrm{L}^2(\mathscr{B})$ yields

$$\begin{aligned} \mathscr{F}^k_{\mathrm{Sp}}\left(G^{\mathrm{I}}_{m,n,j}, 0, 0\right) &= \sqrt{\frac{4m+2n+3}{a^3}} \int_0^a \frac{K^\alpha_n(r)}{\alpha_{\mathrm{M}}(r)} P_m^{\left(0,n+\frac{1}{2}\right)}\left(2\frac{r^2}{a^2} - 1\right)\left(\frac{r}{a}\right)^n \mathrm{d}r\, Y_{n,j}(\xi_k) , \\ \mathscr{F}^k_{\mathrm{Sp}}\left(0, G^{\mathrm{I}}_{m,n,j}, 0\right) &= \sqrt{\frac{4m+2n+3}{a^3}} \int_0^a \frac{K^\beta_n(r)}{\beta_{\mathrm{M}}(r)} P_m^{\left(0,n+\frac{1}{2}\right)}\left(2\frac{r^2}{a^2} - 1\right)\left(\frac{r}{a}\right)^n \mathrm{d}r\, Y_{n,j}(\xi_k) , \\ \mathscr{F}^k_{\mathrm{Sp}}\left(0, 0, G^{\mathrm{I}}_{m,n,j}\right) &= \sqrt{\frac{4m+2n+3}{a^3}} \int_0^a \frac{K^\rho_n(r)}{\rho_{\mathrm{M}}(r)} P_m^{\left(0,n+\frac{1}{2}\right)}\left(2\frac{r^2}{a^2} - 1\right)\left(\frac{r}{a}\right)^n \mathrm{d}r\, Y_{n,j}(\xi_k) . \end{aligned}$$

We will use the abbreviation

$$F_{m,n}(r) := \sqrt{\frac{4m+2n+3}{a^3}} P_m^{\left(0,n+\frac{1}{2}\right)}\left(2\frac{r^2}{a^2} - 1\right)\left(\frac{r}{a}\right)^n, \quad r \in [0,a] .$$

Furthermore, we have

$$\begin{aligned}\mathscr{F}_{\mathrm{Gr}}^{k}\left(G_{m,n,j}^{\mathrm{I}},0,0\right) &= \mathscr{F}_{\mathrm{Gr}}^{k}\left(0,G_{m,n,j}^{\mathrm{I}},0\right)=0\,,\\ \mathscr{F}_{\mathrm{Gr}}^{k}\left(0,0,G_{m,n,j}^{\mathrm{I}}\right) &= \delta_{m0}\frac{4\pi}{2n+1}\sqrt{\frac{a^3}{2n+3}}\left(\frac{a}{|x_k|}\right)^n\frac{1}{|x_k|}Y_{n,j}\left(\frac{x_k}{|x_k|}\right)\,.\end{aligned}$$

By means of these expressions, we are now able to calculate the spline basis functions in (12) and the matrix of the system of linear equations in (13). We assume that $(\delta\alpha,\delta\beta,\delta\rho)\in\mathscr{H}^3$, i.e. we choose $\mathscr{H}_1=\mathscr{H}_2=\mathscr{H}_3$ in accordance with our numerical implementation. Note that, due to the coupled structure of the problem, it is necessary to use a vectorial spline, which involves the calculation of the spline coefficients for the vector $(\delta\alpha,\delta\beta,\delta\rho)$ by dissolving the corresponding whole system of linear equations. However, after having obtained these spline coefficients, we can separately evaluate the expansion of the third component of the spline for plotting $\delta\rho$. For this reason, we only show here the formula of the third component of the spline basis functions associated to the splitting function.

$$\begin{aligned}\left(\mathscr{F}_{\mathrm{Sp}}^{k}\mathfrak{K}(\cdot,s\eta)\right)_3 &= \sum_{m=0}^{\infty}\sum_{n=0}^{\infty}\sum_{j=1}^{2n+1}A_{m,n}^2\left(\mathscr{F}_{\mathrm{Sp}}^{k}\left(0,0,G_{m,n,j}^{\mathrm{I}}\right)\right)G_{m,n,j}^{\mathrm{I}}(s\eta)\\ &= \sum_{m=0}^{\infty}\sum_{n=0}^{\infty}\sum_{j=1}^{2n+1}A_{m,n}^2\int_0^a\frac{K_n^{\rho}(r)}{\rho_{\mathrm{M}}(r)}F_{m,n}(r)\,\mathrm{d}r\,Y_{n,j}(\xi_k)F_{m,n}(s)Y_{n,j}(\eta)\\ &= \sum_{m=0}^{\infty}\sum_{n=0}^{\infty}\frac{2n+1}{4\pi}A_{m,n}^2\int_0^a\frac{K_n^{\rho}(r)}{\rho_{\mathrm{M}}(r)}F_{m,n}(r)\,\mathrm{d}r\,F_{m,n}(s)P_n(\xi_k\cdot\eta)\,,\end{aligned}$$

$s\eta\in\mathscr{B}$. The formulae for the first and second component, respectively, are analogous with α and β, respectively, replacing ρ. Furthermore, we get

$$\begin{aligned}\mathscr{F}_{\mathrm{Gr}}^{k}\mathfrak{K}(\cdot,y) &= \left(0,0,\sum_{m=0}^{\infty}\sum_{n=0}^{\infty}\sum_{j=1}^{2n+1}A_{m,n}^2\left(\mathscr{F}_{\mathrm{Gr}}^{k}\left(0,0,G_{m,n,j}^{\mathrm{I}}\right)\right)G_{m,n,j}^{\mathrm{I}}(y)\right)^{\mathrm{T}}\\ &= \left(0,0,\sum_{n=0}^{\infty}\sum_{j=1}^{2n+1}A_{0,n}^2\frac{4\pi}{2n+1}\sqrt{\frac{a^3}{2n+3}}\left(\frac{a}{|x_k|}\right)^n\frac{1}{|x_k|}Y_{n,j}\left(\frac{x_k}{|x_k|}\right)G_{0,n,j}^{\mathrm{I}}(y)\right)^{\mathrm{T}}\\ &= \left(0,0,\sum_{n=0}^{\infty}A_{0,n}^2\left(\frac{|y|}{|x_k|}\right)^n\frac{1}{|x_k|}P_n\left(\frac{x_k\cdot y}{|x_k|\,|y|}\right)\right)^{\mathrm{T}}\,,\end{aligned}\tag{22}$$

$y \in \mathscr{B}$. Moreover, here are the different types of matrix entries:

$$
\begin{aligned}
\mathscr{F}^i_{\mathrm{Sp}}\mathscr{F}^k_{\mathrm{Sp}}\mathfrak{K} &= \sum_{l=1}^{3}\sum_{m=0}^{\infty}\sum_{n=0}^{\infty}\sum_{j=1}^{2n+1} A^2_{m,n}\left(\mathscr{F}^k_{\mathrm{Sp}}\left(G^{\mathrm{I}}_{m,n,j}\,(\delta_{l\nu})_{\nu=1,2,3}\right)\right)\left(\mathscr{F}^i_{\mathrm{Sp}}\left(G^{\mathrm{I}}_{m,n,j}\,(\delta_{l\nu})_{\nu=1,2,3}\right)\right)\\
&= \sum_{m=0}^{\infty}\sum_{n=0}^{\infty} A^2_{m,n}\left[\left(\int_0^a \frac{K^\alpha_n(r)}{\alpha_{\mathrm{M}}(r)}F_{m,n}(r)\,\mathrm{d}r\right)^2+\left(\int_0^a \frac{K^\beta_n(r)}{\beta_{\mathrm{M}}(r)}F_{m,n}(r)\,\mathrm{d}r\right)^2\right.\\
&\qquad\left.+\left(\int_0^a \frac{K^\rho_n(r)}{\rho_{\mathrm{M}}(r)}F_{m,n}(r)\,\mathrm{d}r\right)^2\right]\frac{2n+1}{4\pi}P_n(\xi_i\cdot\xi_k)\,,\\
\mathscr{F}^i_{\mathrm{Sp}}\mathscr{F}^k_{\mathrm{Gr}}\mathfrak{K} &= \sum_{m=0}^{\infty}\sum_{n=0}^{\infty}\sum_{j=1}^{2n+1} A^2_{m,n}\left(\mathscr{F}^i_{\mathrm{Sp}}\left(0,0,G^{\mathrm{I}}_{m,n,j}\right)\right)\left(\mathscr{F}^k_{\mathrm{Gr}}\left(0,0,G^{\mathrm{I}}_{m,n,j}\right)\right) \qquad (23)\\
&= \sum_{n=0}^{\infty} A^2_{0,n}\int_0^a \frac{K^\rho_n(r)}{\rho_{\mathrm{M}}(r)}F_{0,n}(r)\,\mathrm{d}r\sqrt{\frac{a^3}{2n+3}}\left(\frac{a}{|x_k|}\right)^n\frac{1}{|x_k|}P_n\left(\xi_i\cdot\frac{x_k}{|x_k|}\right)\\
&= \sum_{n=0}^{\infty} A^2_{0,n}\int_0^a \frac{K^\rho_n(r)}{\rho_{\mathrm{M}}(r)}r^n\,\mathrm{d}r\,\frac{1}{|x_k|^{n+1}}P_n\left(\xi_i\cdot\frac{x_k}{|x_k|}\right)\\
&= \mathscr{F}^k_{\mathrm{Gr}}\mathscr{F}^i_{\mathrm{Sp}}\mathfrak{K},\\
\mathscr{F}^i_{\mathrm{Gr}}\mathscr{F}^k_{\mathrm{Gr}}\mathfrak{K} &= \sum_{n=0}^{\infty} A^2_{0,n}\frac{4\pi}{2n+1}\frac{a^3}{2n+3}\left(\frac{a^2}{|x_i|\,|x_k|}\right)^n\frac{1}{|x_i|\,|x_k|}P_n\left(\frac{x_i\cdot x_k}{|x_i|\,|x_k|}\right)\,.
\end{aligned}
$$

We observe that all expressions are series of Legendre polynomials, which can be computed (as truncated series) by the Clenshaw algorithm (see [8]). The Jacobi polynomials can be calculated via the usual recurrence formula (see, for example, [65]) and for the integrals over the interval $[0,a]$ a standard quadrature rule (e.g. the composite trapezoidal rule or Simpson's rule) can be used.

7 Numerical Results

In this section, we present some numerical results of the discussed (vectorial) spline multiresolution method. We start with the inversion of a purely gravitational dataset which gives us the harmonic density of the Earth. Afterwards, we carry out inversions of both synthetic and genuine normal mode data. Finally, we consider a combined inversion of normal mode and gravitational data and discuss the occurring problems.

For the inverse gravimetric problem, we use the NASA GSFC and NIMA joint geopotential model EGM96 (Earth Gravity Model 96, see [35]). EGM96 is a spherical harmonic model of the Earth's gravitational potential complete to degree and order 360.
For the normal mode inversion, we use the structure coefficients and sensitivity kernels from the "Normal Mode Seismology" website by J. Resovsky and M. Ritzwoller ([55]).
The data is assumed to be given on the point grid defined in [21, Example 7.1.9].
We start with an inversion of gravitational data without using normal modes. For this purpose, we take EGM96 from degree 3 up to degree 360. This means that we obtain the harmonic part of the density variation. Figure 2 shows the reconstruction of the density variation $\delta\rho$ on a sphere which is located 0.1%

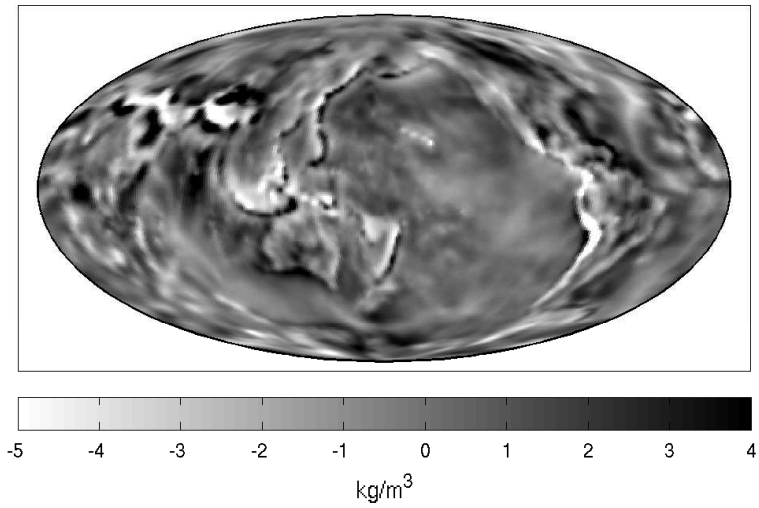

Figure 2: Harmonic density variation shortly below the Earth's surface

below the Earth's surface, i.e. on a sphere with the radius $r = 0.999 \cdot a \approx 6365$ km. For the inversion, we used a CP-scaling function at scale $J = 8$ (see (15)). Note that the obtained spline is a harmonic function due to the structure of the spline basis functions and the restriction to pure gravitational data (see (22)). We can see that many topographical structures at the Earth's surface and some tectonic boundaries are well recognisable in the result.
However, with increasing depth we obtain more and more smoothed versions of the structures at the surface. This is due to the fact that the dominating structure inside the Earth is almost spherically symmetric. The harmonic part of a spherically symmetric density distribution is a constant function (see e.g. [41]). Furthermore, we know from the maximum principle that a harmonic function on the ball $\mathscr{B}$ has its maxima and minima on the boundary of $\mathscr{B}$ (cf. e.g. the results in [45]). These facts confirm that it is absolutely necessary to include also seismic data in our inversions in order to get reasonable solutions in the Earth's interior.
As a next step, we want to test the normal mode inversion on a simple synthetic function. For this purpose, we define

$$\frac{\delta\alpha(r\xi)}{\alpha_{\mathrm{M}}(r)} = \frac{\delta\beta(r\xi)}{\beta_{\mathrm{M}}(r)} = \frac{\delta\rho(r\xi)}{\rho_{\mathrm{M}}(r)} := \mathscr{Y}_{4,2}(\xi)$$

for all $r\xi \in \mathscr{B}$, where $\mathscr{Y}_{4,2}$ is a real fully normalized spherical harmonic. Then we calculate the spherical harmonic coefficients of ten different splitting functions by

$$\sigma_i^{\wedge}(n,j) = \int_0^a \mathbf{k}_{n,i}(r) \cdot \big(\delta\mathbf{m}^{\wedge}(n,j)\big)(r)\,\mathrm{d}r$$

for $n = 2,4,6,\ j = 1,\ldots,2n+1,\ i = 1,\ldots,10$, using the composite trapezoidal rule for 222 points in the interval $[0,a]$ (the index i corresponds to the choice of 10 different normal modes). Afterwards, the calculated coefficients are regarded as the given normal mode data and we try to redetermine the relative density deviation $\delta\rho/\rho_{\mathrm{M}}$ by the vectorial spline multiresolution method. We use a CP-scaling

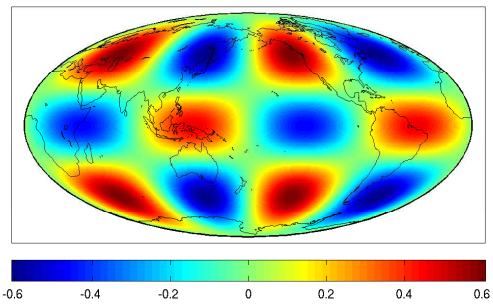

Figure 3: Given density deviation $\delta\rho/\rho_M = \mathscr{Y}_{4,2}$ on the unit sphere

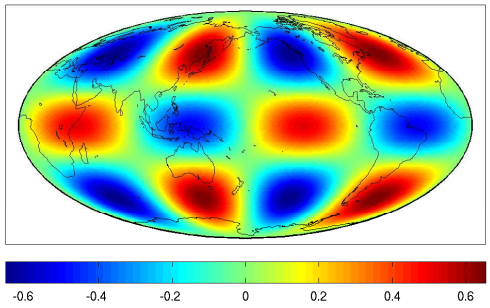

Figure 4: Reconstructed density deviation $\delta\hat{\rho}/\rho_M$ for $r \approx 6365$ km

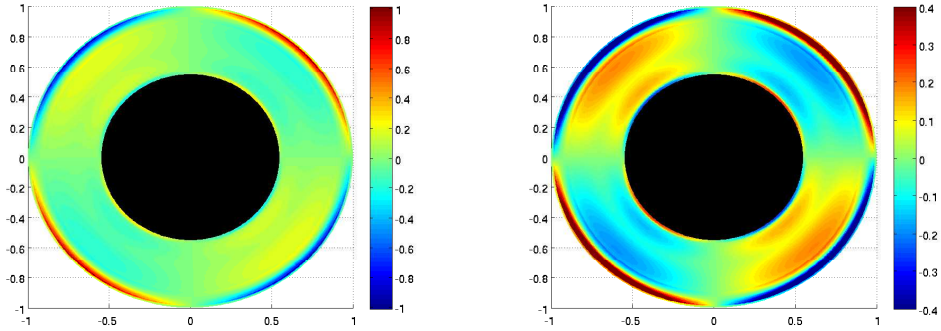

Figure 5: Reconstructed density deviation $\delta\hat{\rho}/\rho_M$ on a cross section in the equatorial plane (with original (left-hand) and adjusted (right-hand) colourbar)

function at scale $J = 9$ (see (15)). Figure 3 shows the given function $\delta\rho/\rho_M = \mathscr{Y}_{4,2}$ on the unit sphere, the result $\delta\hat{\rho}/\rho_M$ is shown in Figure 4 for $r \approx 6365\,\text{km}$. We can see that the result $\delta\hat{\rho}/\rho_M$ has the same spherical structure as the original function $\delta\rho/\rho_M$, except for a change of sign. Figure 5 shows the result $\delta\hat{\rho}/\rho_M$ on a cross section in the equatorial plane, where the Earth's core is blackened. We see that the change of sign does not occur at all depths. Furthermore, we see a high peak at the Earth's surface and a smaller peak at the core-mantle boundary (CMB). We conjecture that certain angular dependencies may be detected qualitatively (maybe even at certain deeper parts of the mantle), whereas the radial dependence probably suffers from the occurrence of phantoms.

Note that we restrict our calculations to the Earth's mantle due to the following considerations. The sensitivity kernels K_n^α, K_n^β and K_n^ρ, $n \in \mathbb{N}_0$ give us the sensitivity of the corresponding multiplet concerning the material properties α, β and ρ in a certain depth. Ideal in the mathematical sense would be functions which are non-zero on the whole interval $[0,a]$. Furthermore, we would like to have functions with varying structure for different multiplets.

However, in reality we do not have such ideal conditions. There are only few known multiplets which are core sensitive, such as the multiplet ${}_8S_1$ (see Figure 6). Moreover, for most of these core sensitive

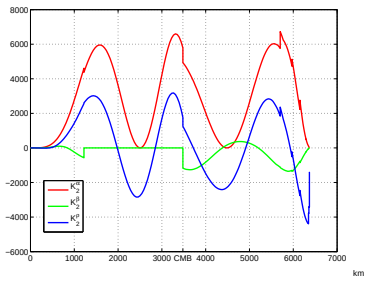

Figure 6: Sensitivity kernels K_2^α, K_2^β, K_2^ρ of multiplet ${}_8S_1$, the horizontal axis refers to the radius r

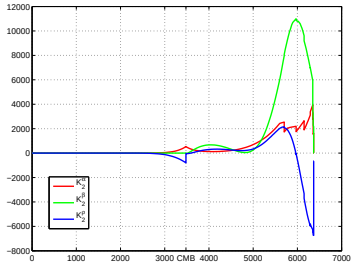

Figure 7: Sensitivity kernels $K_2^\alpha, K_2^\beta, K_2^\rho$ of multiplet ${}_2S_8$

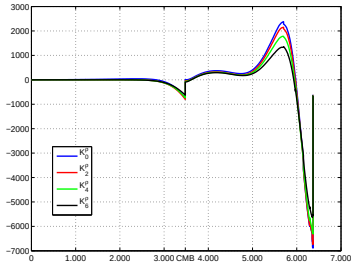

Figure 8: Sensitivity kernels K_0^ρ, K_2^ρ, K_4^ρ, K_6^ρ of multiplet ${}_2S_8$

multiplets only the structure coefficients corresponding to the spherical harmonic degree 2 are known, which is insufficient to obtain satisfying results. For this reason, we use only mantle sensitive multiplets for which the structure coefficients are known at least up to degree 6.

Further numerical tests yield that the resulting splines always have a similar structure with respect to the radius, almost independently from the radial structure of the pre-given density distribution. This result could be a consequence of the fact that many of the applicable sensitivity kernels have a similar structure, comparable to that of the multiplet ${}_2S_8$ (see Figure 7). Note that the structures of the kernels with different degrees corresponding to one multiplet are also similar (see Figure 8). If we consider the kernels K_n^ρ, $n = 0,2,4,6$, in Figure 8 we recognise immediately the structure of the above calculated splines. We have two changes of sign, a high peak at the Earth's surface and a smaller peak at the core-mantle boundary. This result confirms our speculation that the radial structure of the splines reproduces mainly the structure of the sensitivity kernels.

Next we perform an inversion of genuine normal mode data, i.e. the structure coefficients from [55], up to degree 6. This time we calculate the absolute density deviation $\delta\rho$ instead of $\delta\rho/\rho_M$. Again we choose ten different splitting functions, we use a CP-scaling function at scale $J = 5$ (see (15)). The resulting spline S_N is shown for different radii in Figure 9.

Figure 10 shows the result on a cross section in the equatorial plane, where the Earth's core is blackened. Similarly to the synthetic case, we obtain a strong peak at the Earth's surface, then a change of sign and weaker structures. One advantage over the gravity inversion is that we obtain maxima and minima in the interior of the Earth, which is impossible for harmonic functions because of the maximum principle.

In the following, we compare our results to results by other research groups. In [28] and [40], the relative density deviation $\delta\rho/\rho_M$ was also calculated for different radii but with different methods, which motivates a comparison in the search for common structures. In comparison with our spline S_N, we can see that the structure at the radius $r \approx 3600$ km is very similar in [28]. We have an elongate maximum at the pacific region and one at the African continent. Moreover, the distribution of the maxima at the radius $r = 5070$ km obtained in [28] is equal to S_N for $r = 3000$ km. In [40], the result for $r = 5145$ km is comparable to S_N for $r = 3000$ km.

In summary, we can say that the result S_N of our spline interpolation contains some of the structures which were already obtained by other researchers, especially in the deeper mantle regions. In other depths, the

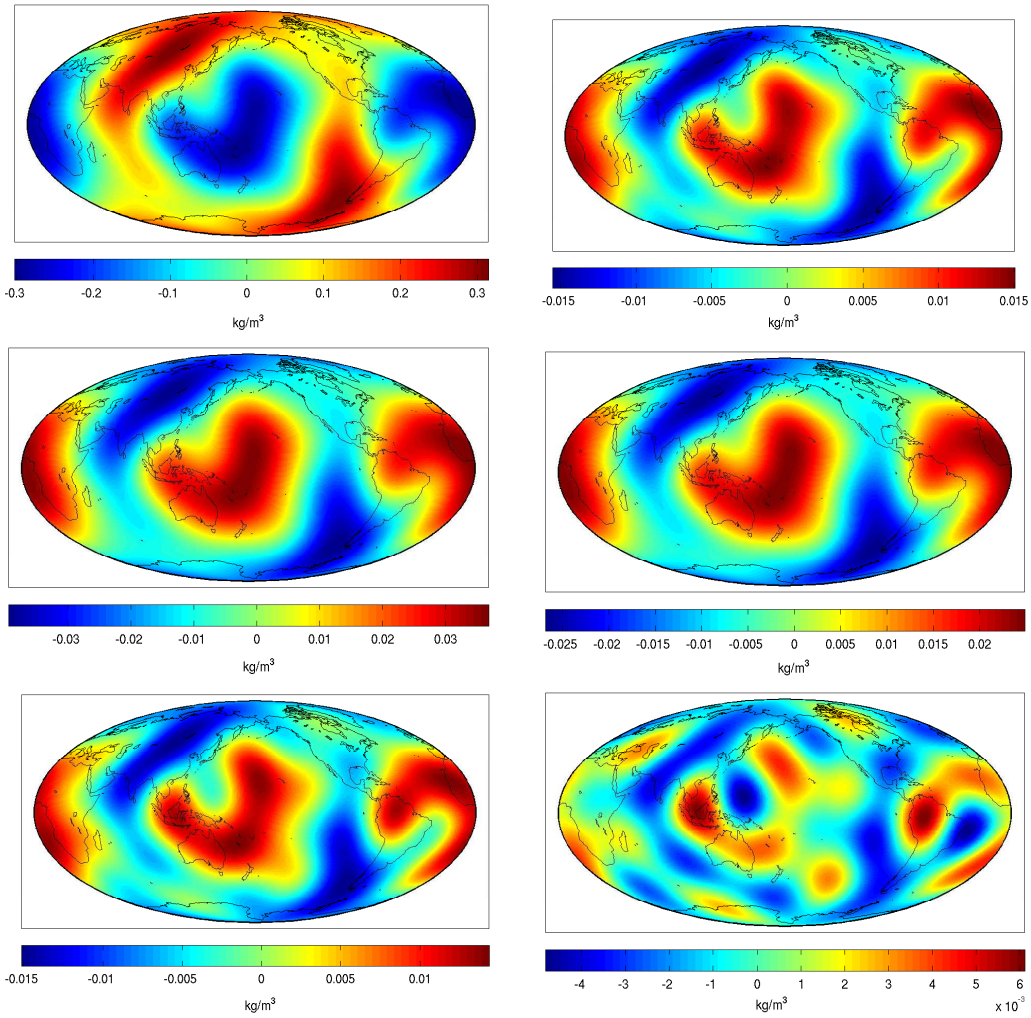

Figure 9: Spline S_N calculated from normal mode data for $r \approx 6365$ km (top left-hand), 5690 km (top right-hand), 5015 km (middle left-hand), 4340 km (middle right-hand), 3670 km (bottom left-hand), and 3000 km (bottom right-hand)

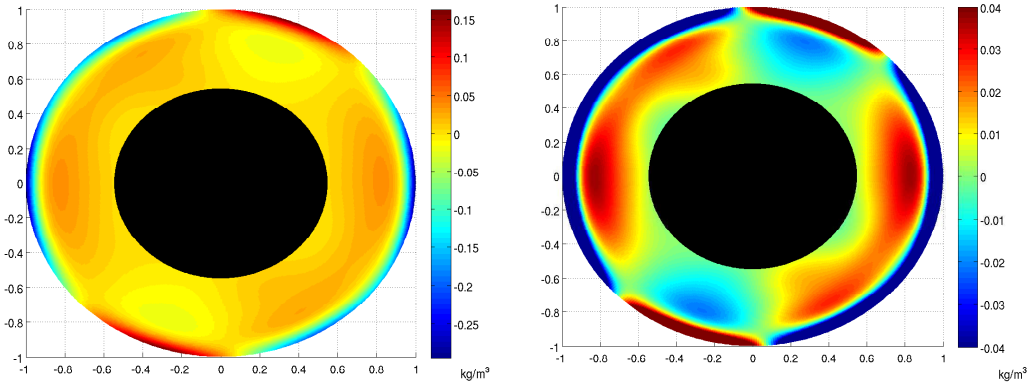

Figure 10: Spline S_N calculated from normal mode data on a cross section in the equatorial plane (with original (left-hand) and adjusted colourbar (right-hand))

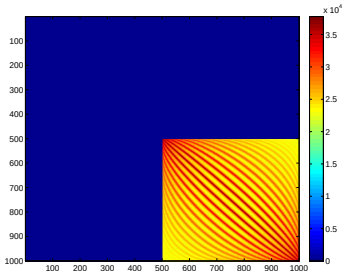

Figure 11: Matrix A

results of the groups differ strongly among each other such that we cannot be sure which results are right (or if any is right). Moreover, it is a highly controversial discussion between seismologists if the current data situation is sufficient for the determination of independent density models.
Finally, we want to carry out a combined inversion of normal mode and gravitational data. For this purpose, we consider at first a small example with one splitting function and the gravitational potential, both evaluated at 500 points on the sphere. We set up the system of linear equations and examine the corresponding matrix which has the form

$$A := \begin{pmatrix} A_1 & A_3^T \\ A_3 & A_2 \end{pmatrix}.$$

The block A_1 corresponds to the splitting function, the block A_2 corresponds to the gravitational potential and the block A_3 is mixed from both (confer (23)). The matrix A is displayed in Figure 11 and we see immediately that it is strongly dominated by the gravitational block A_2. For a better recognition, the blocks are plotted separately in Figure 12.

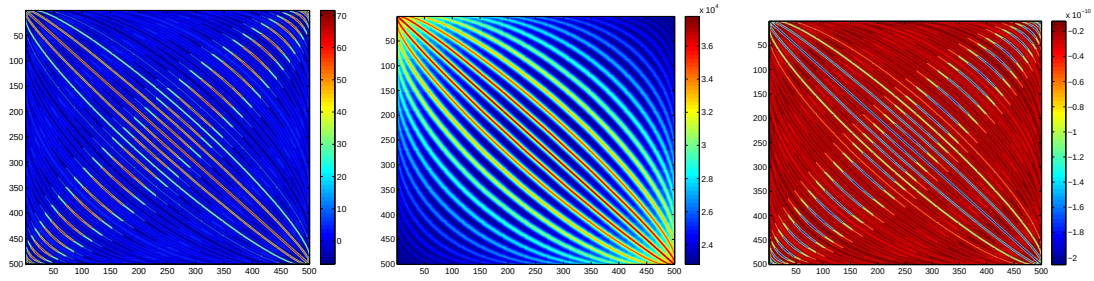

Figure 12: Blocks of the matrix A: A_1 (left-hand), A_2 (middle), A_3 (right-hand)

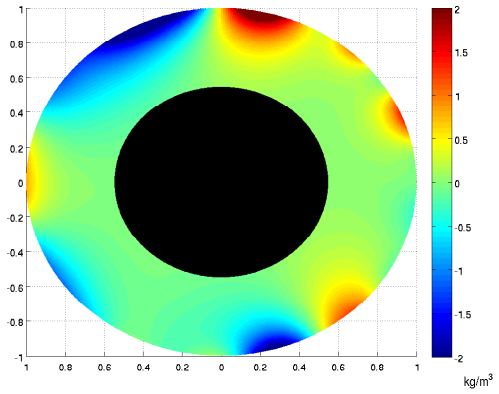

Figure 13: Spline S_{NG} calculated from normal mode and gravitational data on a cross section in the equatorial plane

The matrix and the diagonal blocks have the following conditions:

$$\begin{aligned} \mathrm{cond}(A) &\approx 3 \cdot 10^{21} \\ \mathrm{cond}(A_1) &\approx 4 \cdot 10^{18} \\ \mathrm{cond}(A_2) &\approx 2 \cdot 10^{6} \ . \end{aligned}$$

We realise that the matrix A is very ill-conditioned because of the different sizes of the entries in the blocks. As a method of regularisation, the condition can be improved by weighting the main diagonal (cf. [32]), which is related to the Tikhonov regularisation.
In spite of the problems with the system of linear equations we accomplish now a combined inversion of normal mode and gravitational data. For this purpose, we choose ten different splitting functions and evaluate each of them at 500 points on the sphere. Additionally, we evaluate the gravitational potential at 500 points. In this way, we obtain a matrix which consists of 11×11 blocks. We use a CP-scaling function at scale $J = 5$ (see (15)). The resulting spline S_{NG} is shown on a cross section in the equatorial plane, where the Earth's core is blackened, in Figure 13. Figure 14 shows the result for different radii.

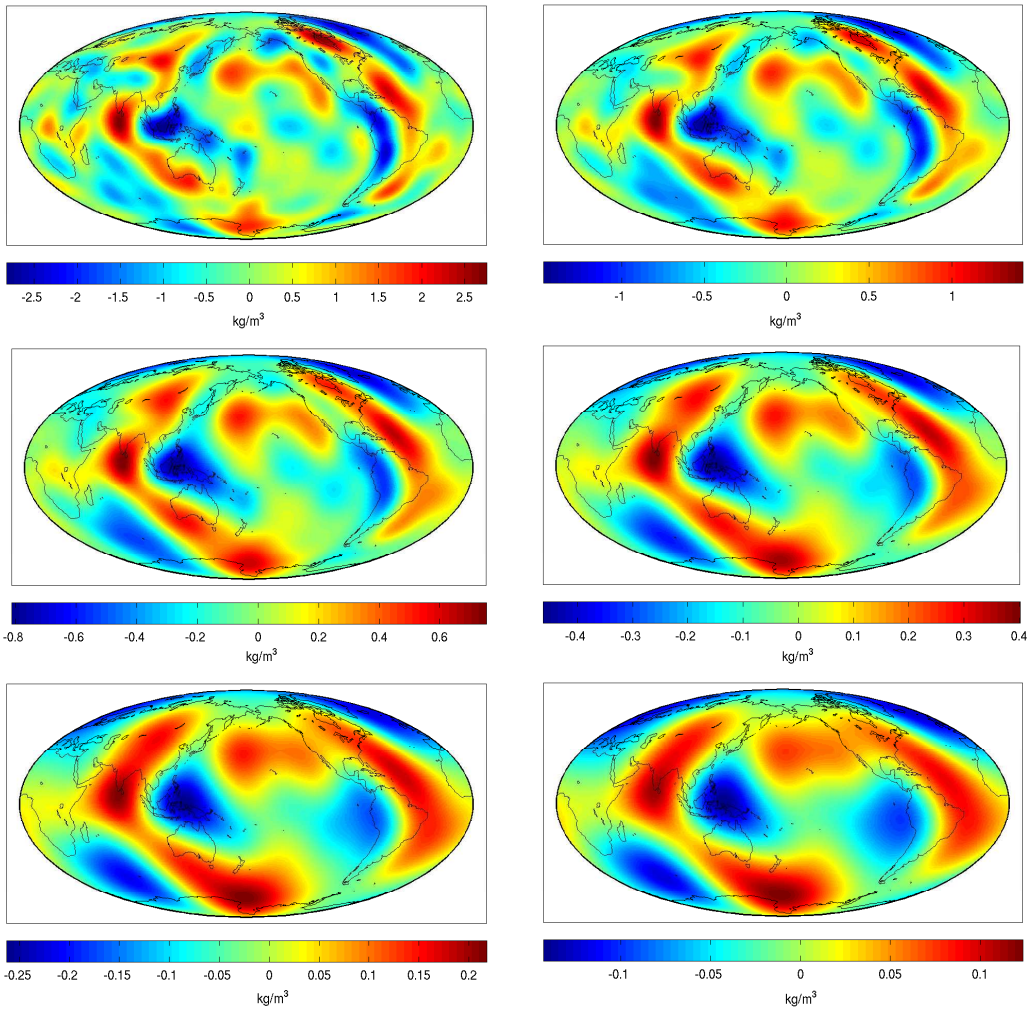

Figure 14: Spline S_{NG} calculated from normal mode and gravitational data for $r \approx 6365$ km (top left-hand), 5690 km (top right-hand), 5015 km (middle left-hand), 4340 km (middle right-hand), 3670 km (bottom left-hand), and 3000 km (bottom right-hand)

8 Outlook: Application of a Matching Pursuit Technique

A particular feature of the proposed method is common to all spline methods. The basis functions of the (scalar) spline $S(x) = \sum_{k=1}^{N} a_k \mathscr{F}^k K_{\mathscr{H}}(\cdot, x),\ x \in \mathscr{B}$, are chosen according to the data structure. This is advantageous if one wants to locally adapt the resolution of the spline to the density of the data grid (see [46]). Using the idea of a matching pursuit in our new approach, we select the basis functions to best match the structure of the solution, which provides us with alternative advantages.

Our method is based on a method developed for a Euclidean setting described in [37] and [66]. We also build a linear expansion $F_N = \sum_{k=1}^{N} \alpha_k d_k$ to approximate the target function F, e.g. the mass density distribution of the Earth. Here, d_k are basis functions that are adaptively and iteratively chosen to best match the signal structure given by the data $y = (\mathscr{F}^1 F, \ldots, \mathscr{F}^M F) =: \mathscr{F}F \in \mathbb{R}^M$ at points $x_1, \ldots, x_M$. In existing variations of the matching pursuit algorithm, the data is always given directly by the target function, i.e. $y = (F(x_1), \ldots, F(x_M))$. However, an extension to a more general setting of bounded linear functionals $\mathscr{F}^k$ (as for the spline method) is possible.

Besides the more beneficial choice of basis functions, there are a few other advantages of using a matching pursuit technique to reconstruct the mass density of the Earth.

Since the basis functions are chosen stepwise, we can directly control the sparsity of the solution and — in contrast to spline methods — we can use results from earlier computations as an intermediate step to zoom in on interesting areas or to improve the solution step by step. We refine the solution by partitioning, for example, South America into four parts. Then we start a new computation in every part where we use the results from earlier computations as an initial approximation F_0 for the solution.

Furthermore, our new method allows us to collect different kinds of basis functions d_k in a so-called dictionary $\mathscr{D}$. We will use the basis functions of the space $\mathrm{L}^2(\mathscr{B})$, defined in Section 2, to cover global trends and we will use localising kernel functions $\{K_h(\cdot, x) \mid h \in]0,1[,\ x \in \mathscr{B}\}$ with varying localisation parameter h and centre points x to represent the detail information. Here,

$$K_h(y,x) = \frac{\tilde{K}_h(y,x)}{\|\tilde{K}_h(\cdot,x)\|_{\mathrm{L}^2(\mathscr{B})}}, \quad x,y \in \mathscr{B}\ ,$$

where

$$\tilde{K}_h(y,x) = \sum_{m=0}^{N_1} \sum_{n=0}^{N_2} \sum_{j=1}^{2n+1} h^{n+m} G^{\mathrm{I}}_{m,n,j}(x) G^{\mathrm{I}}_{m,n,j}(y), \quad x,y \in \mathscr{B}\ .$$

For the implementation, we chose $N_1 = 0$ and $N_2 = 512$.

The basic algorithm is as follows:

We want to choose basis functions d_k and the corresponding coefficients α_k such that they minimise the residual (concerned with the deviation from the data) combined with a regularising penalty term (concerned with the smoothness of the solution), i.e. we want to minimise

$$\sum_{i=1}^{M} (\mathscr{F}^i F_N - y_i)^2 + \lambda ||F_N||^2_{\mathrm{L}^2(\mathscr{B})}\ ,$$

where λ is the regularisation parameter.

We start with $F_0 := 0$. At step $N+1$, we build $F_{N+1} := F_N + \alpha_{N+1} d_{N+1}$ out of F_N such that

$$\sum_{i=1}^{M} \left(\mathscr{F}^i (F_N + \alpha_{N+1} d_{N+1}) - y_i\right)^2 + \lambda \left\|F_N + \alpha_{N+1} d_{N+1}\right\|^2_{\mathrm{L}^2(\mathscr{B})}$$

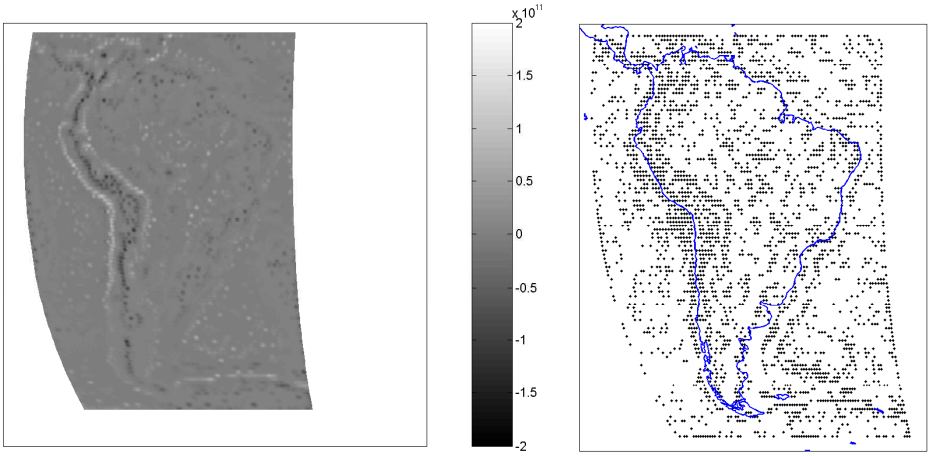

Figure 15: Reconstructed density deviation (left-hand) and centre points x of the chosen basis functions $K_h(\cdot,x)$ (right-hand) computed out of 11,900 data points with 10,000 selected basis functions from the dictionary (i.e. $F_{10,000}$ is shown), $\lambda = 10$, $h \in \{0.95, 0.97, 0.99\}$

is minimised. It can be shown that this task is equivalent to finding (α_{N+1}, d_{N+1}) such that

$$d_{N+1} = \arg\max_{d\in\mathscr{D}} \left| \frac{\langle R_N, \mathscr{F}d\rangle_{\mathbb{R}^M} - \lambda\langle F_N, d\rangle_{\mathrm{L}^2(\mathscr{B})}}{\sqrt{||\mathscr{F}d||^2_{\mathbb{R}^M} + \lambda||d||^2_{\mathrm{L}^2(\mathscr{B})}}} \right| \text{ and}$$

$$\alpha_{N+1} = \frac{\langle R_N, \mathscr{F}d_{N+1}\rangle_{\mathbb{R}^M} - \lambda\langle F_N, d_{N+1}\rangle_{\mathrm{L}^2(\mathscr{B})}}{||\mathscr{F}d_{N+1}||^2_{\mathbb{R}^M} + \lambda||d_{N+1}||^2_{\mathrm{L}^2(\mathscr{B})}},$$

where $R_N = (\mathscr{F}^i F_N - y_i)_{i=1,\dots,M} \in \mathbb{R}^M$ and F_N are given.
The numerical implementation includes, consequently, the computation of the scalar products $\langle R_N, \mathscr{F}d\rangle_{\mathbb{R}^M}$ and $\langle F_N, d\rangle_{\mathrm{L}^2(\mathscr{B})}$ as well as the norms $\|\mathscr{F}d\|^2_{\mathbb{R}^M}$ for all basis functions d in the dictionary $\mathscr{D}$. Note that in our setting the basis functions are normed such that $\|d\|^2_{\mathrm{L}^2(\mathscr{B})} = 1$ for all $d \in \mathscr{D}$. These calculations represent a major part of the computations and can be parallelised. From a computational point of view, this is an important advantage of the presented method.
Figure 15 shows the mass density variations of South America at the Earth's surface computed by our new regularisation method. The given gravitational data was calculated out of EGM96. Obviously, the localised basis functions were chosen according to the structure of the solution, since the data was distributed uniformly. Figure 16 shows the results of a zooming-in, which is first restricted to the north-west of South America and eventually applied to the whole continent. For all three results shown in Figure 16, we started our computations with the results already gained in the computations for Figure 15. Obviously, the resolution is increased in comparison to Figure 15. Note that the same colour scale was used for all three density plots in Figures 15 and 16. Due to the subdivision of the domain during the zooming-in procedure, minor boundary effects occur which have to be controlled by an appropriate weighting process.
Details of the new method will be published in a forthcoming paper. Note that this method also allows

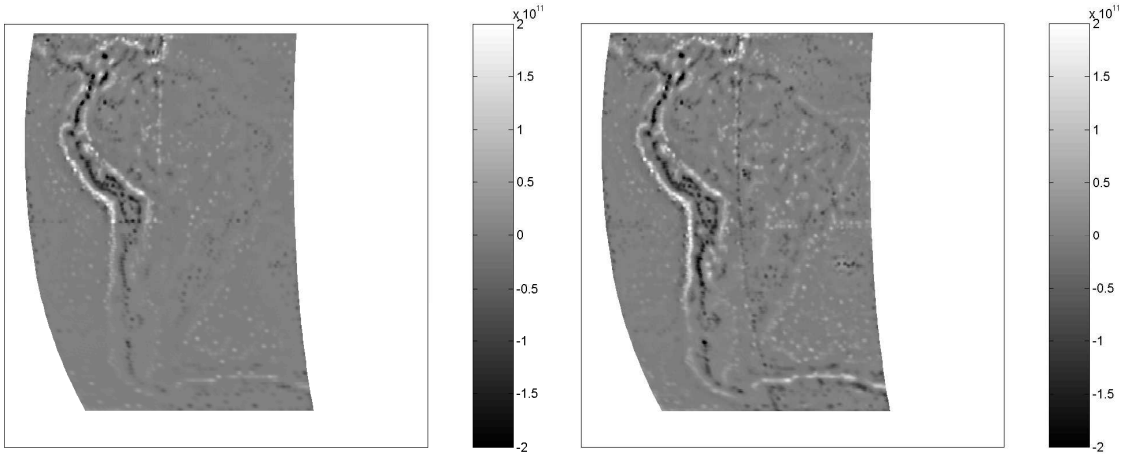

Figure 16: Zooming-in at the north-west of South America (left-hand) and all four sections (right-hand)

the combination of different types of data.

9 Conclusions

The presented spline method is applicable to a joint inversion of gravitational and normal mode anomalies. This combination can reveal some deep mantle structures (in contrast to a pure gravitational inversion). However, a severe non-uniqueness problem remains. More precisely, some lateral variations in the deep mantle might be detectable, whereas the radial structure of the solution is probably dominated by artefacts. Moreover, a strong weighting of normal mode data in comparison to gravitational data is necessary. (Both difficulties are properties of the combined inverse problem and not of the spline method.) Further research on the choice of the weight should be done in the future. Finally, a dictionary-based sparse regularisation technique yields first promising results for the inverse gravimetric problem.

10 Acknowledgments

The authors gratefully acknowledge the support by the German Research Foundation (DFG), projects MI 655/2-1 and MI 655/2-2.

References

[1] A. Amirbekyan and V. Michel, *Splines on the 3-dimensional Ball and their Application to Seismic Body Wave Tomography*, Inverse Problems **24** (2008), 1–25.

[2] A. Amirbekyan, V. Michel, and F.J. Simons, *Parameterizing Surface-Wave Tomographic Models with Harmonic Spherical Splines*, Geophysical Journal International **174** (2008), 617–628.

[3] L. Ballani, J. Engels, and E.W. Grafarend, *Global Base Functions for the Mass Density in the Interior of a Massive Body (Earth)*, Manuscripta Geodaetica **18** (1993), 99–114.

[4] P. Berkel, *Multiscale Methods for the Combined Inversion of Normal Mode and Gravity Variations*, Ph.D. thesis, Geomathematics Group, Department of Mathematics, University of Kaiserslautern, Shaker Verlag, Aachen, 2009.

[5] P. Berkel and V. Michel, *On Mathematical Aspects of a Combined Inversion of Gravity and Normal Mode Variations by a Spline Method*, Schriften zur Funktionalanalysis und Geomathematik **41** (2008), Preprint, Fachbereich Mathematik, TU Kaiserslautern.

[6] F.A. Dahlen and J. Tromp, *Theoretical Global Seismology*, Princeton University Press, Princeton, New Jersey, 1998.

[7] P.J. Davis, *Interpolation and Approximation*, Dover Publications Inc., New York, 1975.

[8] P. Deuflhard, *On Algorithms for the Summation of Certain Special Functions*, Computing **17** (1975), 37–48.

[9] H.M. Dufour, *Fonctions Orthogonales dans la Sphère. Résolution Théorique du Problème du Potentiel Terrestre*, Bulletin Géodésique **51** (1977), 227–237.

[10] European Space Agency (ESA), *European Views on Dedicated Gravity Field Missions: GRACE and GOCE*, ESD-MAG-REP-CON-001, Earth Sciences Division Consultation Document, Noordwijk, 1998.

[11] European Space Agency (ESA), *Gravity Field and Steady-State Ocean Circulation Mission*, ESA SP-1233(1), European Space Agency Publications Division, Noordwijk, 1999.

[12] M.J. Fengler, D. Michel, and V. Michel, *Harmonic Spline-Wavelets on the 3-dimensional Ball and their Application to the Reconstruction of the Earth's Density Distribution from Gravitational Data at Arbitrarily Shaped Satellite Orbits*, Zeitschrift für Angewandte Mathematik und Mechanik (ZAMM) **86** (2006), 856–873.

[13] A.S. Fokas, I.M. Gel-fand, and Y. Kurylev, *Inversion Method for Magnetoencephalography*, Inverse Problems **12** (1996), L9–L11.

[14] A.S. Fokas, Y. Kurylev, and V. Marinakis, *The Unique Determination of Neuronal Currents in the Brain via Magnetoencephalography*, Inverse Problems **20** (2004), 1067–1082.

[15] A.S. Fokas and V. Michel, *Electro-Magneto-Encephalography for the Three-Shell Model: Numerical Implementation for Distributed Current in Spherical Geometry*, Preprint NI09031 of the Isaac Newton Institute for Mathematical Sciences, 2009.

[16] A.M. Forte, A.M. Dziewonski, and R.J. O'Connell, *Continent-Ocean Chemical Heterogeneity in the Mantle Based on Seismic Tomography*, Science **268** (1995), 386–388.

[17] A.M. Forte and J.X. Mitrovica, *Deep-Mantle High-Viscosity Flow and Thermochemical Structure Inferred from Seismic and Geodynamic Data*, Nature **410** (2001), 1049–1056.

[18] W. Freeden, *Multiscale Modelling of Spaceborne Geodata*, Teubner, Stuttgart, Leipzig, 1999.

[19] W. Freeden and T. Gervens, *Vector Spherical Spline Interpolation*, International Series of Numerical Mathematics (ISNM) **90** (1989), 157–171.

[20] W. Freeden and T. Gervens, *Vector Spherical Spline Interpolation (Basic Theory and Computational Aspects)*, Mathematical Methods in the Applied Sciences **16** (1993), 151–183.

[21] W. Freeden, T. Gervens, and M. Schreiner, *Constructive Approximation on the Sphere (With Applications to Geomathematics)*, Oxford University Press, Oxford, 1998.

[22] W. Freeden and V. Michel, *Multiscale Potential Theory (with Application to the Geosciences)*, Birkhäuser, Boston, 2004.

[23] W. Freeden, V. Michel, and H. Nutz, *Satellite-to-Satellite Tracking and Satellite Gravity Gradiometry (Advanced Techniques for High-Resolution Geopotential Field Determination*, Journal of Engineering Mathematics **43** (2002), 19–56.

[24] GeoForschungsZentrum Potsdam (GFZ), *The CHAMP Mission*, `http://op.gfz-potsdam.de/champ`.

[25] GeoForschungsZentrum Potsdam (GFZ), *The GRACE Mission*, `http://op.gfz-potsdam.de/grace`.

[26] D. Giardini, X.-D. Li, and J.H. Woodhouse, *Three-Dimensional Structure of the Earth from Splitting in Free Oscillation Spectra*, Nature **325** (1987), 405–411.

[27] X. He and J. Tromp, *Normal-Mode Constraints on the Structure of the Earth*, Journal of Geophysical Research **87** (1996), 7772–7778.

[28] M. Ishii and J. Tromp, *Normal-Mode and Free-Air Gravity Constraints on Lateral Variations in Velocity and Density of Earth's Mantle*, Science **285** (1999), 1231–1236.

[29] M. Ishii and J. Tromp, *Even-Degree Lateral Variations in the Earth's Mantle Constrained by Free Oscillations and the Free-Air Gravity Anomaly*, Geophysical Journal International **145** (2001), 77–96.

[30] M. Ishii and J. Tromp, *Constraining Large-Scale Mantle Heterogeneity Using Mantle and Inner-Core Sensitive Normal Modes*, Physics of the Earth and Planetary Interiors **146** (2004), 113–124.

[31] T.H. Jordan, *A Procedure for Estimating Lateral Variations from Low-Frequency Eigenspectra Data*, Geophysical Journal of the Royal Astronomical Society **52** (1978), 441–455.

[32] P. Kammann and V. Michel, *Time-Dependent Cauchy-Navier Splines and their Application to Seismic Wave Front Propagation*, Zeitschrift für Angewandte Mathematik und Mechanik (ZAMM) **88** (2008), 155–178.

[33] C. Kuo and B. Romanowicz, *On the Resolution of Density Anomalies in the Earth's Mantle Using Spectral Fitting of Normal Mode Data*, Geophysical Journal International **150** (2002), 162–179.

[34] G. Lauricella, *Sulla Distribuzione della Massa nell'Interno dei Pianeti*, Rendiconti dell'Accademia Nazionale dei Lincei, Roma **21** (1912), 18–26.

[35] F.G. Lemoine, S.C. Kenyon, J.K. Factor, R.G. Trimmer, N.K. Pavlis, D.S. Chinn, C.M. Cox, S.M. Klosko, S.B. Luthcke, M.H. Torrence, Y.M. Wang, R.G. Williamson, E.C. Pavlis, R.H. Rapp, and T.R. Olson, *The Development of the Joint NASA GSFC and NIMA Geopotential Model EGM96*, NASA/TP-1998-206861, NASA Goddard Space Flight Center, Greenbelt, Maryland, USA, 1998.

[36] X.-D. Li, D. Giardini, and J.H. Woodhouse, *Large-Scale Even-Degree Structure of the Earth from Splitting of Long-Period Normal Modes*, Journal of Geophysical Research **96** (1991), 551–577.

[37] S. Mallat, *A Wavelet Tour of Signal Processing*, 2nd ed., Academic Press, San Diego, London, 1999.

[38] G. Masters, G. Laske, H. Bolton, and A. Dziewonski, *The Relative Behavior of Shear Velocity, Bulk Sound Speed, and Compressional Velocity in the Mantle: Implications for Chemical and Thermal Structure*, Earth's Deep Interior: Mineral Physics and Tomography from the Atomic to the Global Scale (S. Karato, A.M. Forte, R.C. Liebermann, G. Masters, and L. Stixrude, eds.), vol. 117, AGU, Washington D.C., 2000, pp. 63–87.

[39] G. Masters, G. Laske, and F. Gilbert, *Autoregressive Estimation of the Splitting Matrix of Free-Oscillation Multiplets*, Geophysical Journal International **141** (2000), 25–42.

[40] G. Masters, G. Laske, and F. Gilbert, *Matrix Autoregressive Analysis of Free-Oscillation Coupling and Splitting*, Geophysical Journal International **143** (2000), 478–489.

[41] V. Michel, *A Multiscale Method for the Gravimetry Problem: Theoretical and Numerical Aspects of Harmonic and Anharmonic Modelling*, Ph.D. thesis, Geomathematics Group, Department of Mathematics, University of Kaiserslautern, Shaker Verlag, Aachen, 1999.

[42] V. Michel, *A Multiscale Approximation for Operator Equations in Separable Hilbert Spaces – Case Study: Reconstruction and Description of the Earth's Interior*, Habilitation thesis, Geomathematics Group, Department of Mathematics, University of Kaiserslautern, Shaker Verlag, Aachen, 2002.

[43] V. Michel, *Regularized Wavelet-Based Multiresolution Recovery of the Harmonic Mass Density Distribution from Data of the Earth's Gravitational Field at Satellite Height*, Inverse Problems **21** (2005), 997–1025.

[44] V. Michel, *Tomography: Problems and Multiscale Solutions*, contribution to the monograph "Handbook of Geomathematics" (W. Freeden, M.Z. Nashed, T. Sonar, eds.), (accepted, 2009).

[45] V. Michel and A.S. Fokas, *A Unified Approach to Various Techniques for the Non-Uniqueness of the Inverse Gravimetric Problem and Wavelet-Based Methods*, Inverse Problems **24** (2008), 045019(25pp).

[46] V. Michel and K. Wolf, *Numerical Aspects of a Spline-Based Multiresolution Recovery of the Harmonic Mass Density out of Gravity Functionals*, Geophysical Journal International **173** (2008), 1–16.

[47] J.-P. Montagner, *Can Seismology Tell us Anything about Convection in the Mantle?*, Review of Geophysics **32** (1994), 115–138.

[48] H. Moritz, *The Figure of the Earth. Theoretical Geodesy and the Earth's Interior*, Wichmann Verlag, Karlsruhe, 1990.

[49] P. Novikoff, *Sur le Problème Inverse du Potentiel*, Comptes Rendus (Doklady) de l'Académie des Sciences de l'URSS **18** (1938), 165–168.

[50] P. Olson, P.G. Silver, and R.W. Carlson, *The Large-Scale Structure of Convection in the Earth's Mantle*, Nature **344** (1990), 209–215.

[51] P. Pizzetti, *Corpi Equivalenti Rispetto alla Attrazione Newtoniana Esterna*, Rendiconti dell'Accademia Nazionale dei Lincei, Roma **18** (1909), 211–215.

[52] P. Pizzetti, *Intorno alle Possibili Distribuzioni della Massa nell'Interno della Terra*, Annali di Matematica Pura ed Applicata, Milano **17** (1910), 225–258.

[53] C. Reigber, H. Lühr, and P. Schwintzer, *Announcement of Opportunity for CHAMP*, CH-GFZ-AO-001, GFZ Potsdam, 2001.

[54] Reference Earth Model Website (REM), *Modes and Surface Waves*, `http://mahi.ucsd.edu/Gabi/rem.dir/surface/rem.surf.html`.

[55] J.S. Resovsky and M.H. Ritzwoller, *Normal Mode Seismology*, `http://phys-geophys.colorado.edu/geophysics/nm.dir/nm.html`.

[56] J.S. Resovsky and M.H. Ritzwoller, *New and Refined Constraints on the Three-Dimensional Earth Structure from Normal Modes below 3 mHz*, Journal of Geophysical Research **103** (1998), 783–810.

[57] J.S. Resovsky and M.H. Ritzwoller, *Regularization Uncertainty in Density Models Estimated from Normal Mode Data*, Geophysical Research Letters **26** (1999), 2319–2322.

[58] J.S. Resovsky and J. Trampert, *Reliable Mantle Density Error Bars: an Application of the Neighbourhood Algorithm to Normal-Mode and Surface Wave Data*, Geophysical Journal International **150** (2002), 665–672.

[59] M.H. Ritzwoller, G. Masters, and F. Gilbert, *Observations of Anomalous Splitting and their Interpretation in Terms of Aspherical Structure*, Journal of Geophysical Research **91** (1986), 10203–10228.

[60] M.H. Ritzwoller, G. Masters, and F. Gilbert, *Constraining Aspherical Structure with Low Frequency Interaction Coefficients: Application to Uncoupled Multiplets*, Journal of Geophysical Research **93** (1988), 6369–6396.

[61] B. Romanowicz, *Can we Resolve 3D Density Heterogeneity in the Lower Mantle?*, Geophysical Research Letters **28** (2001), 1107–1110.

[62] D.P. Rubincam, *Gravitational Potential Energy of the Earth: A Spherical Harmonic Approach*, Journal of Geophysical Research **84** (1979), 6219–6225.

[63] R. Rummel, S. Lange, and A. Schlicht, *GOCE – Neues Weltbild aus der Schwerkraft*, GOCE-Projektbüro Deutschland, 2008.

[64] M.F. Smith and G. Masters, *Aspherical Structure Constraints From Free Oscillation Frequency and Attenuation Measurements*, Journal of Geophysical Research **94** (1989), 1953–1976.

[65] G. Szegö, *Orthogonal Polynomials*, AMS Colloquium Publications, Volume XXIII, Providence, Rhode Island, 1939.

[66] P. Vincent and Y. Bengio, *Kernel Matching Pursuit*, Machine Learning (2002), no. 48, 169–191.

[67] N. Weck, *Zwei Inverse Probleme in der Potentialtheorie*, Mitteilungen aus dem Institut für Theoretische Geodäsie, Universität Bonn **4** (1972), 27–36.

[68] R. Widmer-Schnidrig, *Application of Regionalized Multiplet Stripping to Retrieval of Aspherical Structure Constraints*, Geophysical Journal International **148** (2002), 201–213.

[69] J.H. Woodhouse and F.A. Dahlen, *The Effect of a General Aspherical Perturbation on the Free Oscillations of the Earth*, Geophysical Journal of the Royal Astronomical Society **53** (1978), 335–354.

[70] K. Yosida, *Functional Analysis*, Springer, Berlin, Heidelberg, New York, 1980.

Siegen Preprints on Geomathematics

The preprint series “Siegen Preprints on Geomathematics” was established in 2010. See www.geomathematics-siegen.de for details and a contact address. At present, the following preprints are available:

1. P. Berkel, D. Fischer, V. Michel: *Spline Multiresolution and Numerical Results for Joint Gravitation and Normal Mode Inversion With an Outlook on Sparse Regularisation*, 2010.

Geomathematics Group Siegen
Prof. Dr. Volker Michel

Contact at:
Geomathematics Group
Department of Mathematics
University of Siegen
Walter-Flex-Str. 3
57068 Siegen
www.geomathematics-siegen.de

UNIVERSITÄT SIEGEN